CANCER

PP2A complex disruptor SET prompts widespread hypertranscription of growth-essential genes in the pancreatic cancer cells

He Xu[1,2,3,4]†, Di Wu[1,2,3,4]*†, Mingming Xiao[1,2,3,4]†, Yubin Lei[5], Yalan Lei[1,2,3,4], Xianjun Yu[1,2,3,4]*, Si Shi[1,2,3,4]*

Hyperactivation of the oncogenic transcription reflects the epigenetic plasticity of the cancer cells. Su(var)3-9, enhancer of zeste, Trithorax (SET) was described as a nuclear factor that stimulated transcription from the chromatin template. However, the mechanisms of SET-dependent transcription are unknown. Here, we found that overexpression of SET and CDK9 induced very similar transcriptome signatures in multiple cancer cell lines. SET localized in the transcription start site (TSS)–proximal regions and supported the RNA transcription. SET specifically bound the PP2A-C subunit and induced PP2A-A subunit repulsion from the C subunit, which indicated the role of SET as a PP2A-A/C complex disruptor in the TSS-proximal regions. Through blocking PP2A activity, SET assisted CDK9 to maintain Pol II CTD phosphorylation and activated mRNA transcription. Our findings position SET as a key factor that modulates chromatin PP2A activity, promoting the oncogenic transcription in the pancreatic cancer.

INTRODUCTION

Nonmutational epigenetic reprogramming is increasingly discussed as a driving force in tumorigenesis (*1*–*3*). Several lines of evidence have indicated the existence of global enhancement of transcription that favors the cancer growth. For instance, c-Myc up-regulation has long been identified as a cancer "driver" (*4*, *5*) and c-Myc was found to amplify almost all the mRNA-transcribing genes in cancer cells (*6*). For another example, aberrant activation of super-enhancers, which associated with the hypertranscription of massive critical oncogenes, was observed in multiple cancers (*7*–*15*). Histone acetylation reader BRD4 recruits Cyclin T/CDK9 complex to phosphorylate RNA polymerase II carboxy terminal domain (Pol II CTD) and hence serves as a genome-wide activator of mRNA transcription (*16*–*20*). Intriguingly, bromodomain and extraterminal domain (BET) inhibitors that specifically target BRD4 have shown to be selective antiproliferation compounds in the preclinical treatment of leukemia and solid tumors (*9*, *21*–*23*). In the opposite, protein phosphatase 2A (PP2A), a tumor suppressor, counteracts the BRD4-CDK9 axis to dephosphorylate Pol II C-terminal repeat domain (CTD) and attenuates global hypertranscription (*24*–*26*).

Hyperactivation of the oncogenic transcription reflects the epigenetic plasticity of the cancer cells, and it has been speculated that chromatin status permissive for transcription onset would favor the cancer cells sampling for the fitness genes to promote cell growth (*2*). However, the epigenetic factors that switch the chromatin status to prompt the global hypertranscription remain largely elusive.

The nuclear oncogene Su(var)3-9, enhancer of zeste, Trithorax (SET; also called TAF-I) was first described as a nuclear factor that stimulated transcription from the chromatin template (*27*–*29*). However, it was also purified as a component of INHAT (inhibitor of histone acetyltransferases) complex that negatively regulated histone acetylation (*30*) and also a potent inhibitory protein of PP2A (*31*–*35*). Later, it was found that the acid tail of SET could bind the lysine-rich domain of histones or other proteins to prevent them from being acetylated. So, SET is an "insulator" of protein acetylation (*36*, *37*). Very controversial conclusions had been made regarding the functions of SET in the gene transcription (*38*–*41*). SET was reported to remodel the chromatin structure and facilitated transcription (*28*, *29*, *42*–*45*). SET was also found to integrate chromatin hypoacetylation and transcriptional repression (*46*–*48*).

In search for the driver factors related to the hypertranscription in the pancreatic cancer, we found that SET actually promoted the RNA transcription, which was related to the function of SET as a PP2A-A/C disruptor.

RESULTS

SET supported the RNA transcription

To find out the mechanism underlying the transcriptional reprogramming in the pancreatic ductal adenocarcinoma (PDAC) cells, we searched for the factors that promote the oncogenic transcription. We focused on the clue that BRD4^{-} Cyclin T/CDK9 axis is the pivotal activator in the Pol II–mediated mRNA transcription (*16*, *19*). We speculated that those genes driving the oncogenic transcription were possibly related to the CDK9 axis. So, up-regulation of those genes would render similar transcriptome changes such as CDK9 gain of function. On the basis of this speculation, we searched for the genes that induced the most similar transcriptome changes such as CDK9–overexpression (OE) (the top CDK9-OE–connected genes; fig. S1A) using a transcriptome matching method (*49*, *50*). After overlapping the top 100 CDK9-OE–connected genes with the 303 candidate nuclear oncogenes in the PDAC (those that are up-regulated in the PDAC tissues, essential for PDAC cell growth, and encoding nuclear proteins; fig. S1B), we found only three genes. Among the three genes, we found that overexpression of the nuclear

[1]Department of Pancreatic Surgery, Fudan University Shanghai Cancer Center, Shanghai 200032, China. [2]Department of Oncology, Shanghai Medical College, Fudan University, Shanghai 200032, China. [3]Shanghai Pancreatic Cancer Institute, Shanghai 200032, China. [4]Pancreatic Cancer Institute, Fudan University, Shanghai 200032, China. [5]Key Laboratory of Growth Regulation and Translational Research of Zhejiang Province, School of Life Sciences, Westlake University, 18 Shilongshan Road, Hangzhou, Zhejiang Province 310024, China.
*Corresponding author. Email: wudi@fudanpci.org (D.W.); yuxianjun@fudanpci.org (X.Y.); shisi@fudanpci.org (S.S.)
†These authors contributed equally to this work.

oncogene SET induced the most similar transcriptome phenotype such as CDK9-OE (fig. S1C).

To testify whether SET is involved in the RNA transcription, we constructed the SET–knockout (KO) lines using CRISPR-Cas9 systems in the SET high-expressing PDAC cell line BXPC3 (fig. S1, D and E). We measured the gross transcription rate (with or without CDK9 inhibition) in the control or SET-KO cells by quantifying the ethynyluridine (EU)–labeled nascent RNA after EU pulse labeling (Fig. 1A). Comparing with the control cells, SET-KO cells transcribed significantly less RNA in a given time (Fig. 1B). In the SET-KO cells, the CDK9 inhibition decreased nascent RNA to a lower level than it did in the control cells (Fig. 1B).

More precise sequencing of the nascent RNA with spike-in normalization technology indicated that SET-KO decreased the global nascent mRNA levels same as the CDK9 inhibition (Fig. 1C). Detailed study of the nascent RNA sequencing (RNA-seq) showed that the major part of the nascent RNA, which were down-regulated by CDK9 inhibition in the control cells, would be decreased to a much

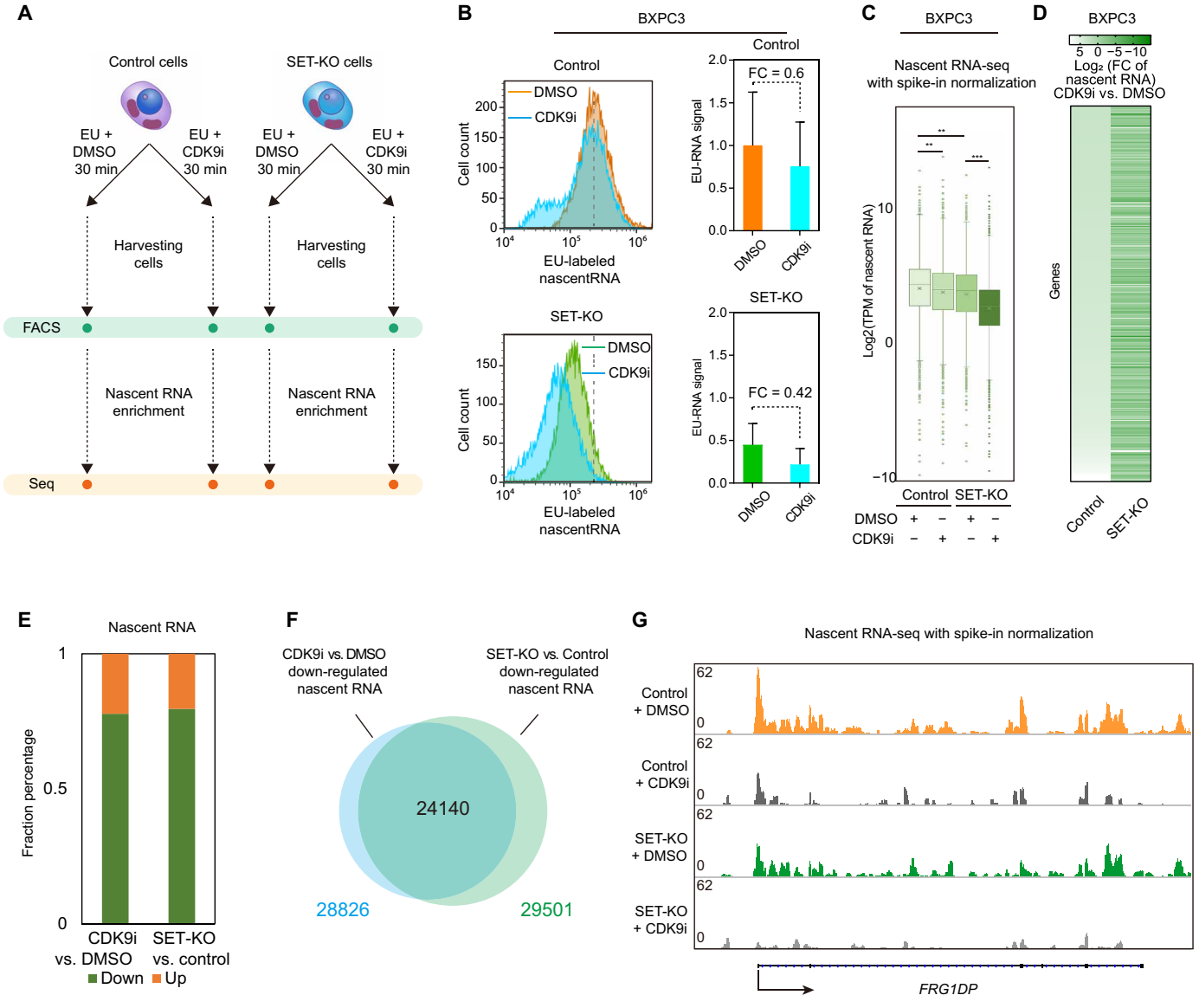

Fig. 1. SET supported the RNA transcription. (**A**) Setup of the experiments to study whether SET is involved in the CDK9-induced transcription. (**B**) BXPC3 control cells or SET-KO cells (treated with or without the CDK9 inhibitor AZD4573 for 2 hours) were pulse-labeled with EU for 30 min, the nascent RNA incorporated with EU was further covalently labeled with fluorescent via Click chemistry, and the labeled cells were analyzed with fluorescence-activated cell sorting. (**C**) Box plot shows the overall changes of nascent RNA in BXPC3 control or SET-KO cells (treated with or without AZD4573). $^{**}P < 0.01$ and $^{***}P < 0.001$. (**D**) Heatmap shows the fold changes of the nascent RNA treated with or without AZD4573 in the BXPC3 control or SET-KO cells; the top down-regulated nascent RNAs in the control cells treated with AZD4573 were shown. (**E**) Fractional bar chart indicates the portion of the down-/up-regulated nascent RNAs in the indicated treatments. (**F**) Venn diagram indicates the overlapping of down-regulated nascent RNAs either after CDK9 inhibitor treatment or after SET-KO. (**G**) Nascent RNA-seq tracks showed the nascent RNA expression in the different treatments at a representative gene locus. FC, fold change.

lower level by CDK9 inhibition in the SET-KO cells (Fig. 1, C and D). Either CDK9 inhibition or SET-KO would suppress nascent mRNA transcription (Fig. 1E), and the bulk of the down-regulated nascent mRNAs either by CDK9 inhibition or by SET-KO were largely overlapped (Fig. 1F), which was quite similar with the phenotype previously observed that CDK9-OE and SET-OE induced the almost same transcriptome changes (fig. S1, A and C). Our discoveries indicated that similar to CDK9, SET also supported the RNA transcription. Also, in the SET-KO cells, CDK9 inhibition was more efficient to reduce the RNA transcription levels (Fig. 1G).

SET localized in the TSS-proximal regions promoting the mRNA transcription

Next, we analyzed the effect of SET-KO upon the stable mRNA level through regular RNA-seq. For the 29,501 genes of which the nascent RNA was decreased in the SET-KO cells versus the control cells, 10,230 of them (~34%) showed down-regulated mRNA in the SET-KO cells (Fig. 2A). To explore more information about the SET target loci in the genome, we performed SET CUT&Tag to identify the genome-wide SET binding sites using a validated SET antibody (Fig. 2C and fig. S1E). We found that the SET-specific signal was

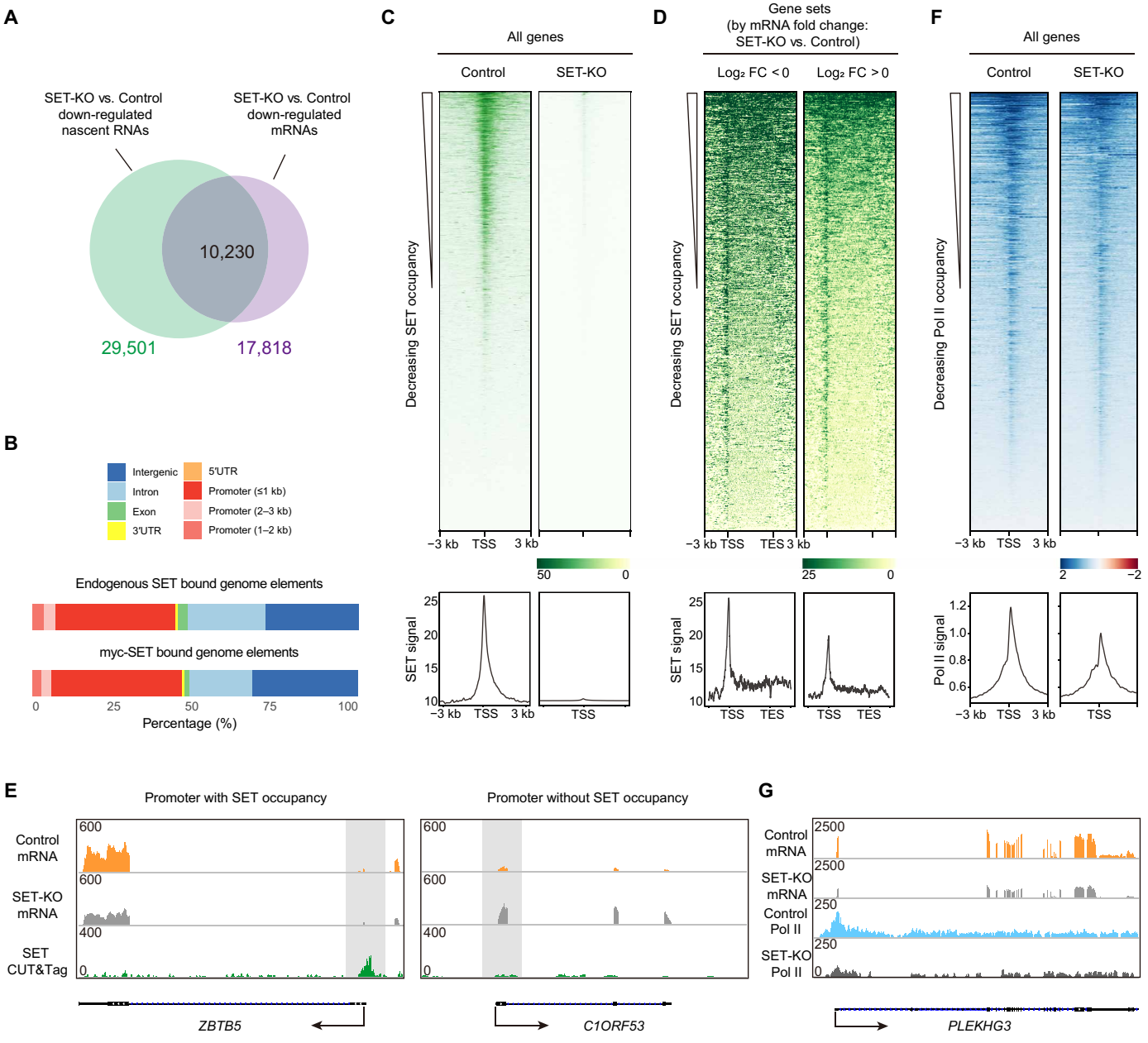

Fig. 2. SET localized in the transcription start sites (TSS)-proximal regions, promoting the mRNA transcription. (**A**) Venn diagram indicates the overlapping of the down-regulated nascent RNA and mRNA in the SET-KO cells versus the control cells. (**B**) SET binding sites within different genomic elements. (**C**) Heatmaps and metaplots of SET CUT&Tag signals in the TSS-proximal regions in the control and SET-KO cells. (**D**) Heatmaps and metaplots of SET CUT&Tag signals in the different gene groups. (**E**) mRNA expression and SET chromatin occupancy at representative gene loci. (**F**) Heatmaps and metaplots show the Pol II ChIP-seq signals at scaled TSS-proximal regions ranked by decreasing occupancy. (**G**) mRNA expression and Pol II chromatin occupancy at a representative gene locus in the control and SET-KO cells.

distributed in the genes and intergenic regions. Approximately 40 to 50% of the SET binding peaks localized in the gene promoter regions (Fig. 2B). Especially, we identified SET binding signals in the transcription start site (TSS)–proximal regions of more than 50% of all genes (Fig. 2C).

Furthermore, to assess whether the TSS occupancy of SET had any relationship with the gene expression level, we grouped the differentially expressed genes (DEGs) after SET-KO into different subsets according to the mRNA fold changes. We found that the down-regulated genes after SET-KO had bound more SET in the control cells (Fig. 2, D and E). It means that the genes directly targeted by SET are inclined to be turned down after SET-KO (Fig. 2D and fig. S2A), which further validated SET gene's function as promoting mRNA transcription. Similarly, the up-regulated genes in the SET-OE cells had more SET binding than the down-regulated genes (fig. S2B). It is noteworthy that the most down-regulated genes in the SET-KO cells had the lower CERES scores, which implies that SET preferred to support the growth-essential genes to transcribe (fig. S2C).

Pol II chromatin immunoprecipitation sequencing (ChIP-seq) analysis showed that, comparing with those in the control cells, Pol II in the TSS-proximal regions was significantly decreased in the SET-KO cells (Fig. 2, F and G). However, in the control and SET-KO cells, as well as in different subset of genes, we found no differences in the Pol II traveling ratio (TR) indexes (fig. S2D). It seemed that SET-KO had induced a substantial decrease of available Pol II engaged to the chromatin, preventing the transcription initiation steps.

SET bound to PP2A-C subunit and repelled PP2A-A from PP2A-C

To elucidate the mechanism of SET gene's function in supporting CDK9-induced and Pol II–mediated transcription, we decided to analyze the binding partners of SET. Using the co-immunoprecipitation–mass spectrum (co-IP MS), we identified the SET binding proteins in two different cell lines (Fig. 3B). In the human embryonic kidney (HEK) 293T cells, SET bound to multiple factors involved in the RNA metabolism and gene expression (fig. S3A) but not CDK9 or Pol II (Rpb1) (Fig. 3B). In the Panc02 cells, SET co-IP enriched CDK9 but still not Pol II (Rpb1) (Fig. 3B). So, there is no evidence that SET interacts with Pol II (Rpb1). Also, the interaction between SET and CDK9 seemed not consistent across different cell lines. Therefore, we inferred that SET might modulate CDK9 and Pol II function through a third mediator.

PP2A complex, consisting of the scaffold subunit A, the regulatory subunit B, and the catalytic subunit C, has been validated to counteract the CDK9 to dephosphorylate Pol II CTD and suppress the global transcription (*24*–*26*). Because SET has been verified as an inhibiting factor of PP2A activity (Fig. 3A) (*31*–*35*). It is strongly implicated that chromatin-associated SET might support CDK9 function through PP2A modulation.

Two different models have been proposed to explain how SET inhibits PP2A:

(model A) SET directly binds PP2A-C and inhibits PP2A-C catalytic activity (*35*, *51*). In this model, SET directly binds PP2A-C subunit but not B or A subunit (*51*), which is in accordance with our data (Fig. 3, B and C).

(model B) SET, as a dimer, directly binds PP2A-B (B56 subunit) but not PP2A-C and modulates PP2A holoenzyme activity in the lung cancer cell lines (*52*, *53*). However, in either HEK293T cells or PDAC cell line Panc02, we found no evidence that SET bound PP2A-B (Fig. 3B).

Actually, through comparing the SET binding proteins in the two cell lines we tested, we found that PP2A-C is a consistent binding protein of SET (fig. S3B).

Although our data supported the model A that SET inhibits PP2A only through the binding with PP2A-C, the molecular details of the mechanism in the model A was still not elucidated completely. The precise formation of PP2A-A/C core enzyme is critical for the PP2A holoenzyme activity and substrate specificity (*54*). Therefore, we conjectured that excessive SET binding to PP2A-C might pose some effect on the formation of PP2A complex.

We constructed a series of truncated or deleted mutations in both SET and PP2A-C proteins (Fig. 3D), trying to map the interaction domains in SET and PP2A-C. Full-length SET bound to PP2A-C and did interrupt the PP2A-A/C interaction (Fig. 3E, arrow head). However, if a stretch of C-terminal domains in SET protein were deleted (SET-ΔC1 or SET-ΔC2), the truncated SET would hardly bind PP2A-C (Fig. 3, E and F). Meanwhile, neither SET-ΔC1 nor SET-ΔC2 mutation would disrupt PP2A-A/C interaction (Fig. 3, E and F). These results highlighted the importance of SET C-terminal domains in binding PP2A-C and impeding PP2A-A/C interaction. Using similar method, we mapped a PP2A-C region (amino acids 207 to 309) that is critical for PP2A-C binding with SET (Fig. 3G). Applying the AlphaFold2-based protein complex simulations, we predicted a structural model of SET: PP2A-C interaction (fig. S3C). In this model, an evolutionarily conserved domain just adjacent to the SET C-terminal acid tail directly binds to a conserved region of PP2A-C (fig. S3, C and D). According to this model, the SET bound with PP2A-C would induce a steric effect that interferes with PP2A-A/C interaction (Fig. 3H and fig. S3C). PP2A-A/C interaction is the foundation for the formation of PP2A/B/C holoenzyme and the full PP2A activity. So, it is possible that SET inhibits PP2A activity through disrupting the PP2A-A/C interaction (Fig. 3H). In accordance with this model, SET mutations with deletion of C-terminal domains showed substantially decreased binding with PP2A-C and no longer disrupted PP2A-A/C interaction or full PP2A activity (Fig. 3, E, F, and I).

SET-KO did not alter the TSS occupancy of CDK9 or PP2A-C but increased PP2A-A localization in the TSS-proximal regions

According to the model above (Fig. 3H), we speculated that chromatin associated SET would induce the repulsion of PP2A-A from the chromatin-bound PP2A-C, hence, to inhibit the PP2A-A/C core enzyme activity in the chromatin. We inferred that SET-KO would stop the repulsion of PP2A-A from PP2A-C and recruit the PP2A-A back to the chromatin-bound PP2A-C.

Western blotting showed that there were no notable changes in the protein expression levels of CDK9, PP2A-A, or PP2A-C in the SET-KO cells versus the control cells (Fig. 4A). So, we performed the spike-in normalized ChIP-seq of CDK9 and PP2A-C and the spike-in normalized CUT&Tag of PP2A-A in the control or SET-KO cells to testify whether SET-KO would change the genomic localization of these factors. Our ChIP-seq data demonstrated that CDK9, PP2A-A, and PP2A-C all localized in the TSS-proximal regions (Fig. 4, B to D). SET-KO had little or no effects on the TSS-bound CDK9 (Fig. 4B) or PP2A-C (Fig. 4, D and E).However, compared to the control cells, TSS-bound PP2A-A was significantly increased in

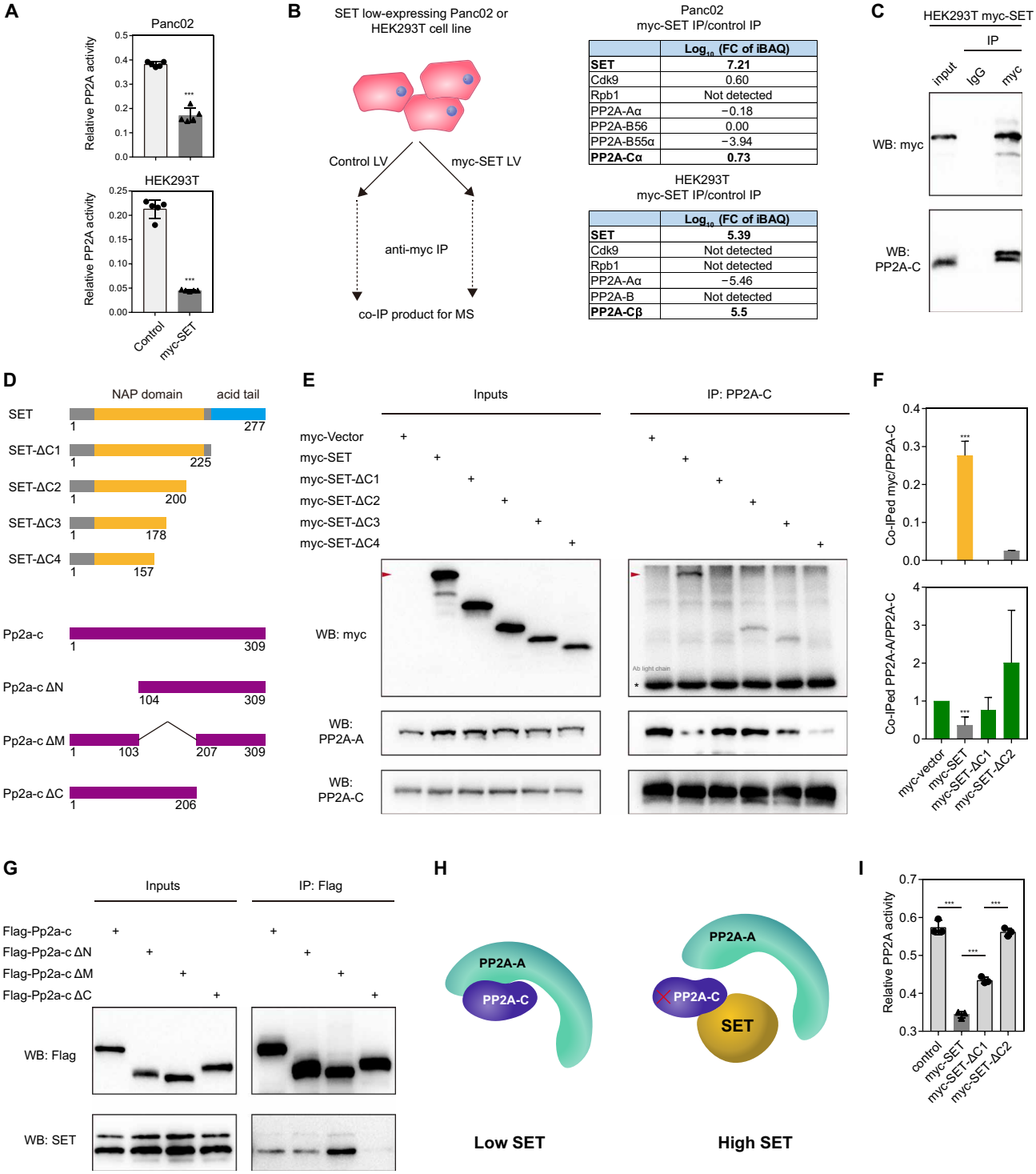

Fig. 3. SET bound to PP2A-C subunit and repelled PP2A-A from PP2A-C. (**A**) The gross PP2A activity was measured in the control or SET-OE cells. ***$P < 0.001$. (**B**) Experimental setup for the SET IP-MS. The table shows the SET-IP enriched and nonenriched proteins. (**C**) Western blot of the co-IP product in the HEK293T SET-OE cells. IgG, immunoglobulin G. (**D**) Illustration of the truncated mutations of SET and Pp2a-c protein. (**E**) Western blot of the co-IP product in the HEK293T cells stably transfected with wild-type SET or various truncated mutations. Also, the blotting bands were quantified using ImageJ software to calculate the relative amount of the co-IPed myc-SET as in the (**F**) top panel or the co-IPed PP2A-A by PP2A-C in the (F) bottom panel. ***$P < 0.001$. (**G**) Western blot of the co-IP product in the HEK293T cells stably transfected with wild-type Pp2a-c or various truncated mutations. (**H**) Mode of action that SET repels PP2A-A from PP2A-C. (**I**) Gross PP2A activity was measured in the HEK293T cells stably transfected with wild-type SET or different truncated mutations. ***$P < 0.001$. WB, Western blot.

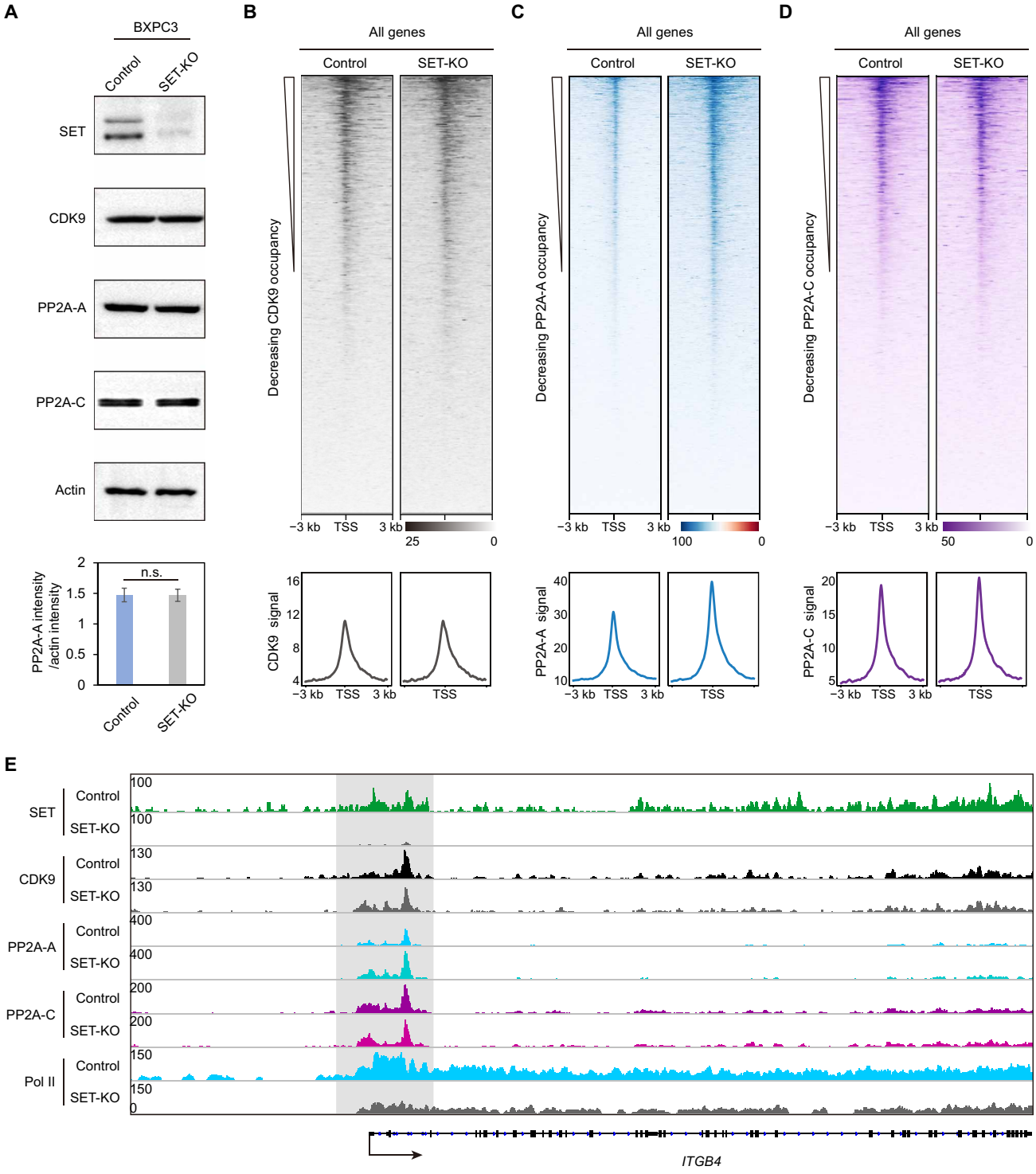

Fig. 4. SET-KO did not alter the TSS occupancy of CDK9 or PP2A-C but increased PP2A-A localization in the TSS-proximal regions. (**A**) Western blotting in the control and SET-KO cells, and the quantification of the PP2A-A protein levels according to the actin levels as the internal control. n.s., not significant. (**B** to **D**) Heatmaps and metaplots of CDK9, PP2A-A, and PP2A-C binding signals in the TSS-proximal regions in the control and SET-KO cells. (**E**) Overlaid CUT&Tag and ChIP-seq tracks showed the chromatin occupancy of SET, CDK9, PP2A-A, PP2A-C, and Pol II at a representative gene locus in the control and SET-KO cells.

the SET-KO cells (Fig. 4, C and E). These results supported the model that SET induced the PP2A-A repulsion from the chromatin-associated PP2A-C. Intriguingly, a recent paper has reported that another cellular PP2A inhibitor protein CIP2A also binds to the PP2A trimer and resulted in the dislocation of the PP2A-A subunit from the complex (*55*). The interesting parallel of this paper with our research indicated that PP2A-A repulsion could be common mechanistic basis for PP2A inhibition by its inhibitory proteins.

SET regulated Pol II CTD phosphorylation through modulating PP2A activity

The fully phosphorylated Pol II CTD [YSPT(S/T)P(T/K)] repeats is necessary for the activation of Pol II–mediated transcription (*16*–*19*). Pol II CTD is phosphorylated by CDK9 and dephosphorylated by chromatin associated PP2A. We have demonstrated that SET might be a functional inhibitor of chromatin PP2A. So, we further examined whether SET could promote Pol II CTD phosphorylation.

In a recent research that has systematically studied the phosphoproteome changes after SET loss of function, MS-based screen was applied to compare the phosphoproteins in the SET–knockdown (KD) cells versus the control cells (*56*). In their published data, we found that SET-KD specifically decreased the phosphorylation of Pol II CTD domain in the fifth serine positions (Pol II S5-p) (fig. S4A). Using Western blotting, we confirmed that phosphorylated Pol II, especially the Pol II S5-p, was significantly decreased in the SET-KO cells compared with the control cells (Fig. 5, A, B, and D).

Since that SET did not show consistent interaction with CDK9 (Fig. 3B) and that SET-KO did not change the CDK9 protein level or CDK9 localization in the TSS-proximal regions (Fig. 4, A and B), SET is more likely to affect Pol II CTD S5-p by modulating the dephosphorylation process of Pol II CTD. In the control and SET-KO cells, we inhibited CDK9 activity and detected the stability of Pol II S5-p in the course of time. We found in the SET-KO cells that the Pol II S5-p level dropped more quickly than that in the control cells (Fig. 5, A and C), which indicated that Pol II CTD dephosphorylation process was strengthened in the SET-KO cells. These results indicated that chromatin PP2A activity might be elevated in the SET-KO cells.

To test whether SET modulated Pol II S5-p level through PP2A, we pretreated the control and SET-KO cell with or without PP2A inhibitor and detected the Pol II S5-p level using Western blot. We found that if PP2A activity was blocked, SET-KO would not decrease the Pol II S5-p level (Fig. 5D). These results demonstrated that SET maintains Pol II S5-p level via blocking PP2A activity.

To investigate whether SET promoted transcription through disrupting PP2A, we also pretreated the control and SET-KO cell with or without PP2A inhibitor and detected the mRNA expression level using RNA-seq. Actually, in the LB100-treated cells where PP2A activity was blocked, SET-KO could no longer reduce the gene expression as it did in the PP2A normal cells (Fig. 5, E and F).

In detail, we analyzed the effects of PP2A inhibition on mRNA transcriptome in both control and SET-KO cells. We found that, for the most decreased oncogenes in the SET-KO cells including *EGFR*, *MET*, and *ZBTB5*, PP2A long time inhibition (~24 hours) will increase their mRNA levels (fig. S4B). For all the down-regulated genes in the SET-KO cells versus the control cells, 67.5% of them were eventually up-regulated by PP2A inhibition (fig. S4C).

We also found that SET not only bound with PP2A-C but also colocalized with PP2A-C along the genome (Fig. 5G). PP2A-C and SET even cotargeted the similar genome DNA motifs (fig. S4D). These facts highlighted the possibility that SET could support Pol II phosphorylation by the in situ inhibition of chromatin-associated PP2A (Fig. 5H).

SET was essential for the PDAC disease progression and tumor growth

SET was reported to be a nuclear oncoprotein (*57*, *58*). Immunohistochemistry (IHC) staining using SET-specific antibody revealed increasing nuclear signal in the PDAC tissues other than the adjacent noncancer tissues (Fig. 6A). Patient cohort study verified that higher SET protein levels predicted poor outcomes and shorter survival time (Fig. 6B). Via CRISPR-Cas9 technology and stable transfection, we have constructed SET loss-of-function and gain-of-function lines in different PDAC cells (fig. S1, D and E). In vitro studies demonstrated that growth rate and colony formation rate were both decreased in the SET-KO PDAC cells but increased in the SET-OE cells (Fig. 6, C and D). In vivo experiments also showed that the growth rate of the SET-KO PDAC xenografts was decreased comparing with the control (Fig. 6, E and F).

Oncogene *MET* is a direct transcriptional target of SET and PP2A

In search of the Achilles' heel in the SET-overexpressing cancers, we analyzed the correlation between the drug sensitivity and the SET expression level in multiple cancer cell lines (Fig. 7A) using the National Cancer Institute's CTD^2 drug sensitivity database (*59*). Statistically, we found that cancer cells with higher SET expression levels showed higher vulnerability to some compounds with various cellular targets (fig. S5A), especially the Taxels and the c-Met inhibitor tivantinib (Fig. 7A and fig. S5B). We conformed that comparing to the SET-KO cells, the SET-expressing control cells were more sensitive to the c-Met inhibitor tivantinib (Fig. 7, B and C).

c-Met is encoded by the oncogene *MET*. We found that SET and PP2A-C colocalized in the TSS-proximal region of the *MET* (Fig. 7D). Compared with the control cells, the SET-KO cells showed unchanged PP2A-C but significant increased PP2A-A occupancy in the TSS-proximal region of the *MET* (Fig. 7D). In concert, Pol II engagement in the *MET* was decreased and the *MET* mRNA level was suppressed in the SET-KO cells (Fig. 7D). We further validated that c-Met protein level was decreased by SET-KO (Fig. 7E). SET and c-Met expression level were positively correlated in the cancer cells or in the PDAC samples (fig. S5, C to E). These observations demonstrated that *MET* is a direct transcriptional target of SET and PP2A complex.

We pretreated the control and SET-KO cell with or without PP2A inhibitor and detected the *MET* mRNA levels using the reverse transcription quantitative polymerase chain reaction (RT-qPCR). We found that when PP2A activity was blocked, SET-KO could no longer decrease the *MET* mRNA (Fig. 7F). These results indicated that SET promoted the transcription of *MET* through the inhibition of PP2A.

Increased SET was correlated with the Pol II activation and c-Met overexpression in the PDAC samples

The Pol II CTD S5-p is a hallmark of Pol II activation and transcription initiation (*10*, *15*). In our cohort of patients with PDAC, we found that the Pol II S5-p level was increased in the PDAC tissues (fig. S5F). High Pol II S5-p level was correlated with shorter survival time in PDAC (fig. S5G), reflecting the hyperactive oncogenic transcription in the PDAC tissues.

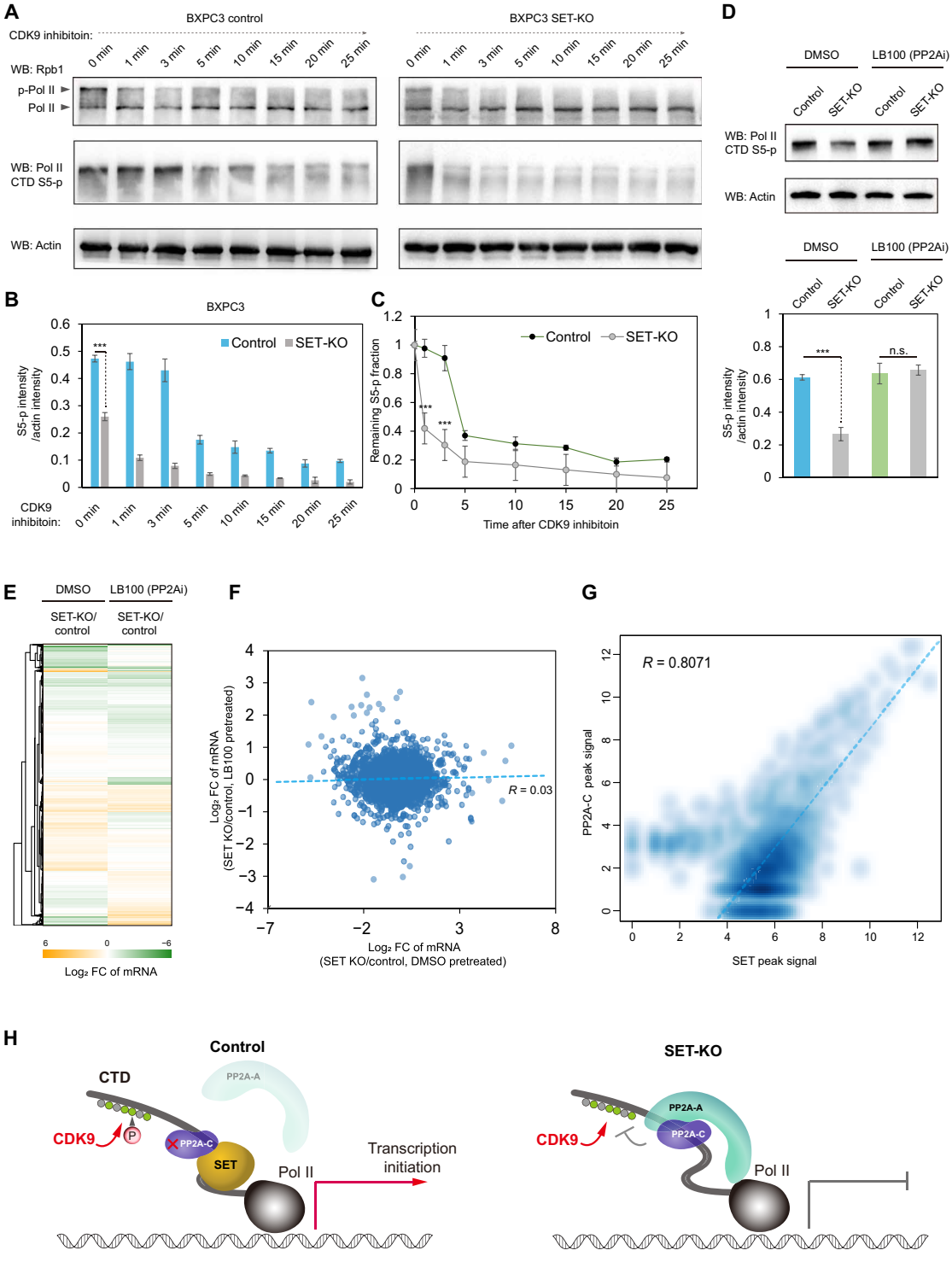

Fig. 5. SET regulated Pol II CTD phosphorylation through modulating PP2A activity. (**A**) BXPC3 control or SET-KO cells were treated with the CDK9 inhibitor AZD4573. After the CDK9 inhibition, cell samples were collected at different time points. Also, these cell lysate samples were subjected to Western blotting. (**B**) Blotting bands in (A) were quantified using ImageJ software to calculate the relative amount of the Pol II S5-p. ***$P < 0.001$. (**C**) Relative amount of the Pol II S5-p in the control or SET-KO cells at different time points were renormalized according to that at the starting time point (0 min). ***$P < 0.001$. (**D**) Western blot of the cell extract of BXPC3 control and SET-KO after treatment with dimethyl sulfoxide (DMSO) or the PP2A inhibitor LB100 for 24 hours. Also, the relative Pol II S5-p levels were quantified. ***$P < 0.001$. (**E**) Heatmap and (**F**) scatterplot shows the mRNA fold changes of the DEGs in the SET-KO cells versus the control cells, with or without the pre-inhibition of PP2A activity. (**G**) Density plot shows the correlation between the SET and PP2A-C binding sites along the genome. (**H**) Model diagram explains that SET, directly inhibiting the chromatin-associated PP2A, regulated Pol II CTD phosphorylation and transcriptional activation.

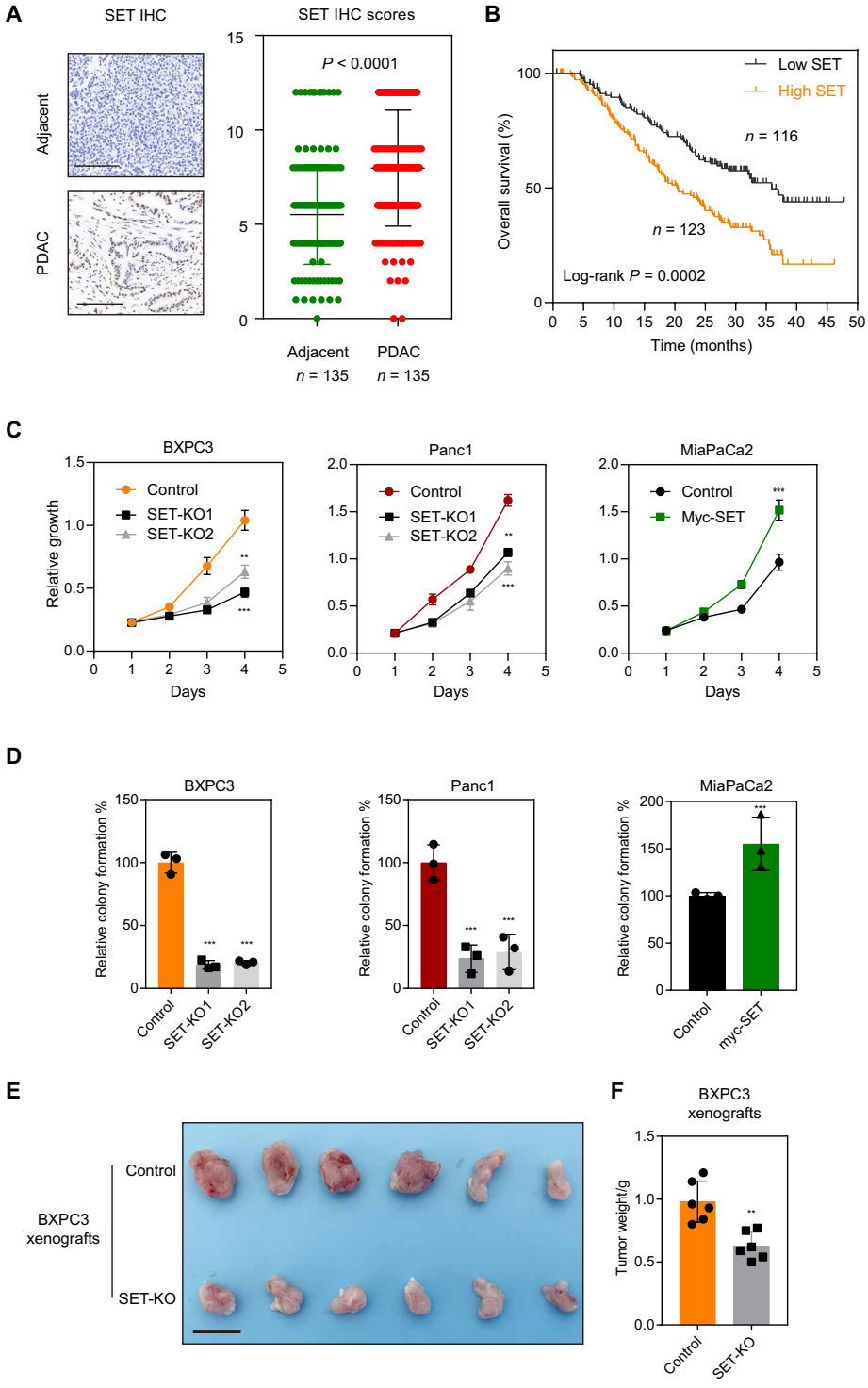

Fig. 6. SET was essential for the PDAC disease progression and tumor growth. (**A**) IHC using SET-specific antibody in the PDAC tissue sections. Scale bars, 200 μM. The right plot chart shows SET IHC score in the PDAC tissues versus the adjacent nontumor tissues. (**B**) On the basis of the SET IHC scores, a cohort of 239 patients with PDAC was divided into SET high and SET low groups, and the survival plot was drawn. (**C**) Growth curve and (D) colony formation rate of SET-KO or SET-OE cell lines compared with the control cells. $^{**}P < 0.01$ and $^{***}P < 0.001$. (**E**) BXPC3 control cells or SET-KO cells were subcutaneously implanted into the nude mice for 28 days before (**F**) the xenograft tumor weight was measured. $^{**}P < 0.01$.

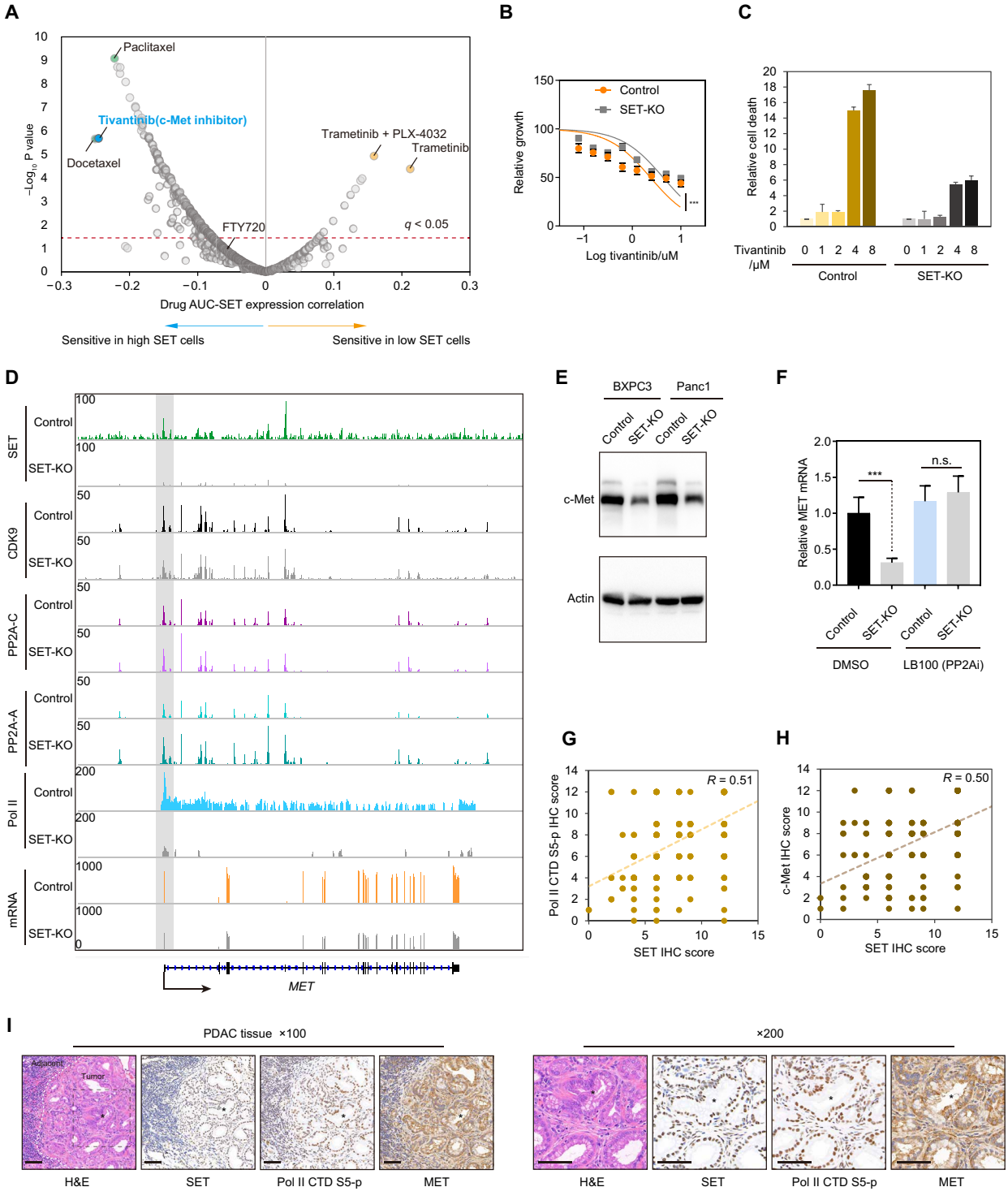

Fig. 7. Oncogene *MET* is a direct transcriptional target of SET and PP2A. (**A**) Scatter plot shows the relationship between the SET expression level in different cancer cell lines and the cell sensitivity to different drugs These data are derived from the National Cancer Institute's CTD^2 drug sensitivity database (*59*) (**B**) Drug IC_{50} assay was carried out in the control and SET-KO cells. ***$P < 0.001$. (**C**) Cell death assay after c-Met inhibitor treatment was carried out in the control and SET-KO cells. (**D**) Overlaid CUT&Tag, ChIP-seq, and RNA-seq tracks showed the SET, CDK9, PP2A-A, PP2A-C, and Pol II chromatin occupancy, as well as the mRNA expression, at the *MET* gene locus in the control and SET-KO cells. (**E**) Western blot of the cell extract of the control and SET-KO cells. (**F**) We pretreated the control and SET-KO cell with DMSO or the PP2A inhibitor LB100 for 24 hous and detected the MET mRNA levels using the RT-qPCR. ***$P < 0.001$. (**G**) Scatterplot indicates the correlation between SET IHC score and Pol II CTD S5p IHC score or (**H**) between SET IHC score and c-Met IHC score in the PDAC tissues. (**I**) Representative IHC images. Scale bars, 50 μM. The star marks the same position in the tissue. H&E, hematoxylin and eosin.

We found in the PDAC tissue samples that Pol II S5-p level was positively correlated with the SET expression level (Fig. 7G). The *MET* expression was also elevated in the PDAC (fig. S5H). We observed that *MET* high expression was correlated with short survival time of patients with PDAC (fig. S5, I and J) in accordance with previous reports (*60*–*64*).

The increased c-Met was positively correlated with Pol II S5-p level and the SET level (Fig. 7H and fig. S5K). In conclusion, IHC study in the PDAC consecutive sections (Fig. 7I) supported the hypothesis that overexpressed SET, supporting CDK9-induced Pol II CTD phosphorylation, prompts the hypertranscription of growth-essential genes including the oncogene *MET*.

Treating the PDAC cells with FTY720

The ceramide analogs including FTY720 have been reported to bind SET and block SET dimerization (*52*, *53*). It is believed that FTY720 inhibits the binding of SET with PP2A (*52*). According to these, FTY720 would be the perfect compound to treat SET-positive PDAC.

However, as the drug sensitivity experiments showed, the median inhibitory concentration (IC_{50}) of FTY720 is above 10 μM for 21 of the 28 PDAC cell lines tested (fig. S6A). Unlike the c-Met inhibitor tivantinib, which showed increased drug sensitivity in the cells expressing higher level of SET, FTY720 drug sensitivity appeared not significantly correlated with the SET expression level (Fig. 7A and fig. S6B).

If FTY720 inhibits cell growth via inhibiting SET in the PDAC cells, then it should be expected that FTY720 will not inhibit the growth of the isogenic SET-KO cells. However, compared to the control cells, SET-KO cells were more sensitive to the FTY720 (fig. S6C).

We have demonstrated that MET is one direct target gene of SET and PP2A. However, FTY720 could not modulate the MET expression levels in the control or SET-KO isogenic cells (fig. S6D).

The results above showed that FTY720 seemed not a plausible candidate drug to treat PDAC and whether FTY720 inhibited PDAC cells through SET still requires further investigation.

SET and PP2A directly regulated the expression of CBP/p300, which promoted the enhancer histone acetylation and the enhancer activation

SET modulated global histone acetylation levels and landscapes, which are also related to the transcription (fig. S7, A to C). Generally, the introns and the genomic loci with higher histone acetylation tended to lose H4 acetylation after SET-KO (fig. S7C and S7D). These facts prompt us to study whether histone acetyltransferases were regulated by SET.

We found that SET and PP2A-C colocalized in the TSS-proximal regions of *EP300* and *CBP*, which encode the important histone acetyltransferase CBP/p300 (Fig. 8, A and B). In the SET-KO cells, PP2A-C occupancy was not significantly changed, while more PP2A-A was recruited into the TSS-proximal regions of *EP300* and *CBP* (Fig. 8, A and B), which validated the role of SET as a PP2A-A/C complex disruptor in the TSS-proximal regions of these two genes.

The mRNA levels of *EP300* and *CBP* were decreased in the SET-KO cells comparing with the control cells (Fig. 8, A and B). We pretreated the control and SET-KO cell with or without the PP2A inhibitor and detected the *EP300* and *CBP* mRNA levels using the RT-qPCR. We found that when PP2A activity was blocked, SET-KO could no longer decrease the *EP300* or *CBP* mRNA (Fig. 8, C and D). These results indicated that SET promoted the transcription of *EP300* and *CBP* through the inhibition of PP2A.

We used the western blotting to detect CBP protein levels and performed the CUT&Tag assays to detect the CBP genomic binding loci in the control and SET-KO cells. We found that CBP protein levels were reduced, and the enhancer occupancy of CBP was decreased in the SET-KO cells (Fig. 8, E and F). With less CBP bound to the enhancer regions, the enhancer histone H4 acetylation levels were decreased in the SET-KO cells (Fig. 8G).

The SET-KO cells exhibited down-regulated histone H4 acetylation with decreased Pol II occupancy in the super-enhancers (fig. S7, E and F) and less enhancer RNA transcribed from the super-enhancers (fig. S7G). All these indicated the inactivation of the super-enhancers.

Actually, compared with the control cells, SET-KO cells had fewer number of super-enhancers (Fig. 8H). Many super-enhancers in the control cells are associated with receptor tyrosine kinase (RTK) or AKT signaling pathway genes (including *MET* and *EGFR*; Fig. 8I). When the super-enhancer activity was attenuated by SET-KO, those RTK genes with other growth-promoting genes were also turned down (Fig. 8H). The super-enhancers play a prominent role in orchestrating oncogene expression selectively (*9*). Our results demonstrated that SET directly regulated CBP/p300 transcription via antagonizing PP2A. Through promoting the CBP/p300 expression level, SET might indirectly induce the enhancer activation and the enhancer related oncogenic transcription, which might in turn reinforce the direct activation of oncogene transcription (Fig. 9).

DISCUSSION

Our results indicated that, as a disruptor of PP2A-A/C complex, SET is able to promote CDK9-induced Pol II phosphorylation, eventually activating transcription. Pol II CTD is dynamically phosphorylated by CDK9 and dephosphorylated by the chromatin-associated PP2A. SET binds to the PP2A-C in the TSS-proximal regions, repelling the PP2A-A from the PP2A-C and inhibiting the PP2A-A/C core enzyme activity in the TSS-proximal regions. So, the overexpressed SET shifts the balance between Pol II CTD phosphorylation and dephosphorylation, increased the Pol II CTD phosphorylation and mRNA transcription (Fig. 5H). Hence, it is explainable that SET-OE had similar effects on cell transcriptome such as the CDK9-OE (fig. S1, A and C).

In the SET-KO cells, PP2A-A is no longer repelled from the PP2A-C. So, the PP2A-A and PP2A-C subunit are restored to form PP2A-A/C core enzyme in the TSS-proximal regions. Hence, the PP2A activity is increased in the TSS-proximal regions. Under this condition, the dephosphorylation rate of Pol II CTD will also increase. When CDK9 was inhibited, the gross dephosphorylation rate of Pol II CTD is higher in the SET-KO cells than in the control cells. So, the Pol II transcriptional activity will drop faster in the SET-KO cells after CDK9 inhibition. It explains why CDK9 inhibition in the SET-KO cells would render the nascent RNA transcription to a lower level than in the control cells (Fig. 1, B to D).

Pol II S5-p was reported to be related to transcription initiation, while S2-p is more significant in the transcription elongation after Pol II pausing (*17*, *65*, *66*). Although our results showed that SET-KO induced significant decrease of Pol II S5-p, we did not observe obvious differences in Pol II pausing in SET-KO cells versus the control cells. Instead, we only observed a significantly decreased Pol II binding in the TSS-proximal regions of the SET-KO cells. So, it seems that SET loss of function is not 100% identical with the PP2A gain of function.

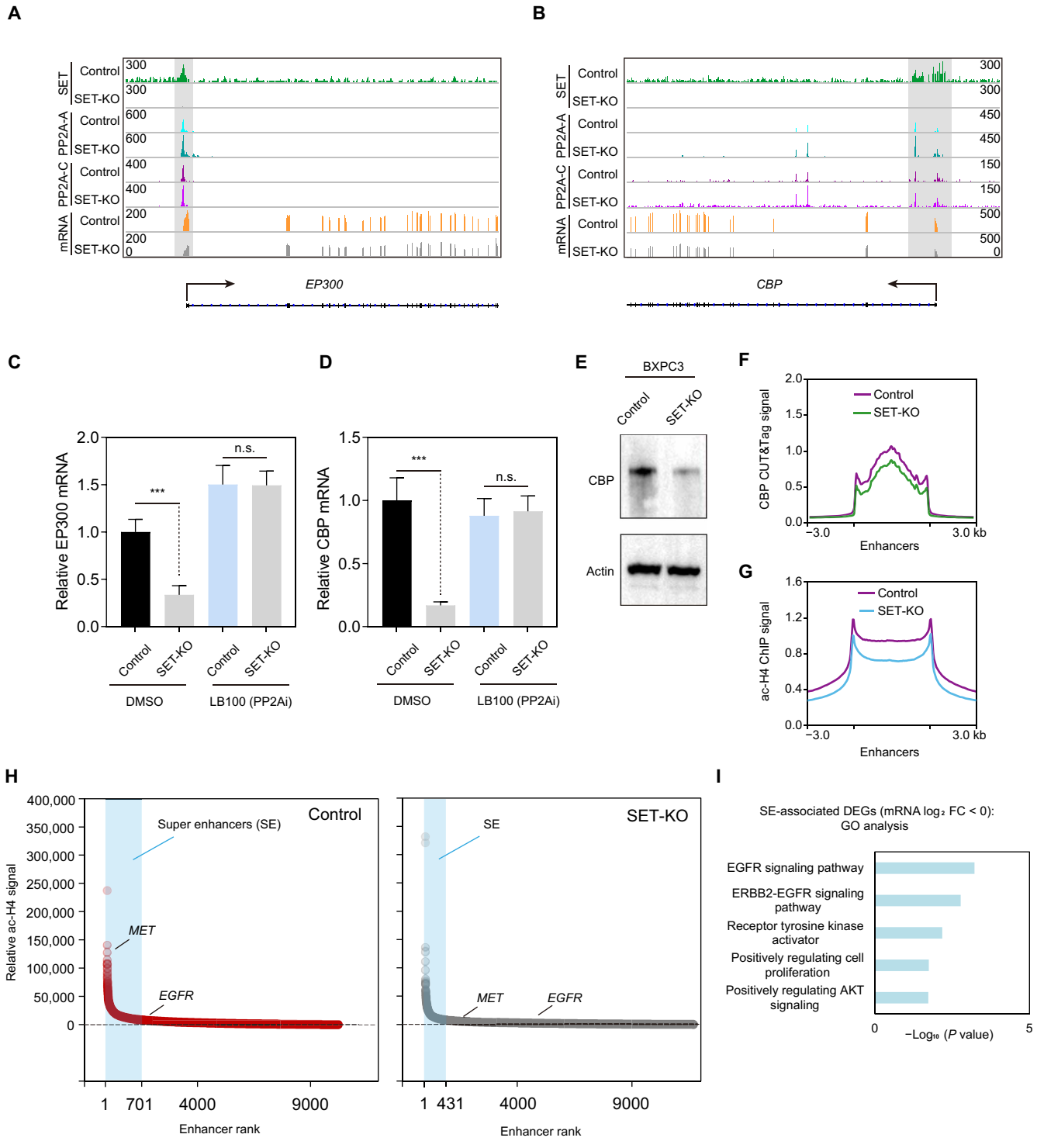

Fig. 8. SET and PP2A directly regulated the expression of CBP/p300, which promoted the enhancer histone acetylation and the enhancer activation. (**A**) Overlaid ChIP-seq, CUT&Tag, and RNA-seq tracks showed the chromatin occupancy of SET, PP2A-A, and PP2A-C, as well as the mRNA expression at the *EP300* gene or (**B**) at the *CBP* gene in the control and SET-KO cells. (**C**) We pretreated the control and SET-KO cell with DMSO or the PP2A inhibitor LB100 for 24 hours and detected the *EP300* mRNA levels using the RT-qPCR. ***$P < 0.001$. (**D**) We pretreated the control and SET-KO cell with DMSO or the PP2A inhibitor LB100 for 24 hours and detected the *CBP* mRNA levels using the RT-qPCR. ***$P < 0.001$. (**E**) Western blotting in the control and SET-KO cells. (**F**) Metaplots show the CBP occupancy or (**G**) Histone H4 acetylation signals in the enhancer regions in the control or SET-KO cells. (**H**) Scatterplot depicts the ranking of all the enhancers in the control or SET-KO cells, according to the enhancer histone acetylation levels. Super-enhancers (SEs) were identified with the ROSE program. Enhancers (including super-enhancers) were associated with the nearest gene within 50 kb. (**I**) GO analysis was done for the down-regulated DEGs associated with the reduced super-enhancer in the SET-KO cells versus the control cells. EGFR, endothelial growth factor receptor.

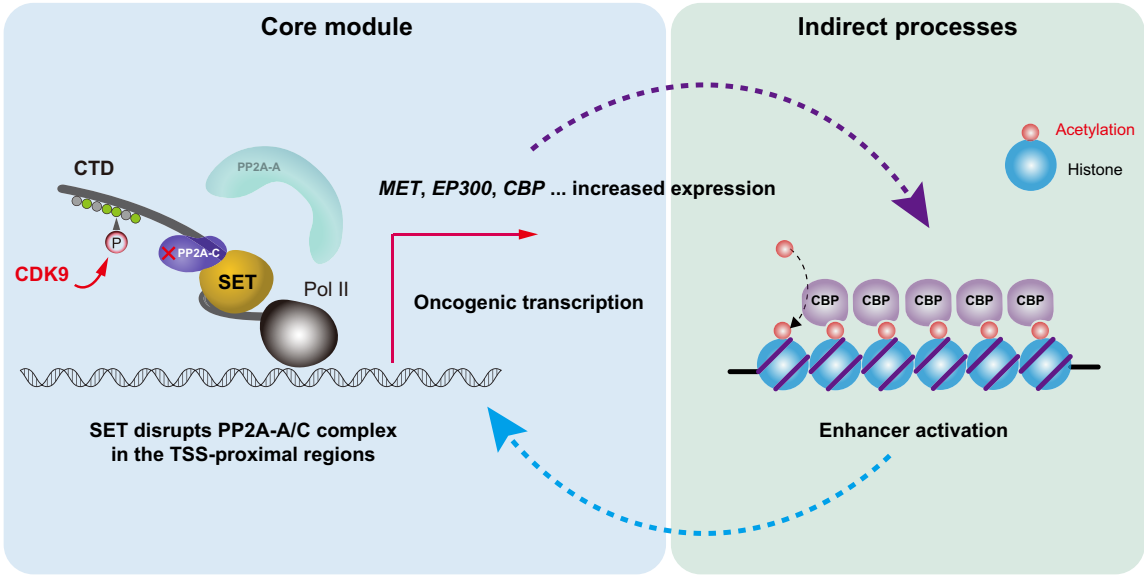

Fig. 9. The working model of the SET induced oncogenic transcription. The core module: SET directly inhibits the PP2A in the TSS-proximal regions, which is the core of the mechanism underlying the SET-induced oncogenic transcription. Through this mechanism, SET directly targets *MET*, *EP300*, and *CBP*, etc. The indirect processes: SET up-regulates the P300/CBP expression, which locates in the enhancer regions as the histone acetyltransferase. Increased CBP activates the enhancers, which further activate the oncogenic transcription.

SET was reported to be a histone chaperone with possible chromatin remodeling activity (*28*, *29*, *67*, *68*). We suspect that SET-KO might also induce chromatin restriction to directly hinder the Pol II engagement to the chromatin. This effect could overlap with SET's function as a PP2A inhibitor to jointly affect the transcription. Under this scenario, SET loss would suppress transcription initiation so profoundly that its effects on transcription elongation are difficult to be observed.

Especially, we found that oncogene *MET* is one of the direct downstream targets of SET-induced oncogenic transcription. Relative study in the PDAC patient cohort and previous studies all suggested that *MET* might contribute to the malignancy of PDAC (*63*, *69*–*71*). Our results added to the pharmaceutical value of c-Met inhibitors in the treatment of SET-positive PDAC (*72*–*76*).

EP300 and *CBP* are another two direct targets of SET. Through promoting CBP/p300 expression, SET indirectly boosted the enhancer histone acetylation and the activation of enhancer-related oncogene. This process seemed to be an indirect, secondary mechanism that SET used to promote the oncogenic transcription. However, it is working compatibly with SET's core function as a chromatin PP2A inhibitor.

Although we have found that CBP/p300 is the linkage between SET and the enhancer histone acetylation, we could not rule out other mediators or alternative mechanisms underlying the SET-induced histone acetylation remodeling. In the light of recent phosphoproteome data that SET/PP2A regulates the phosphorylation of dozens of chromosomal and epigenetic proteins including HDACs (*56*, *77*), it is noteworthy for the readers to understand that SET has also a broader role in regulating phosphorylation of protein involved in transcription and epigenetics, which might also eventually contribute to the landscape of histone acetylation and other modifications.

Limitations of the study

We found that SET is important for the Pol II function and transcription initiation. However, we could not certify the effects of SET on the transcription elongation or other down-stream events because SET-KO induced a profound loss of Pol II engagement to the TSS-proximal regions, which might mask SET's effects on other down-stream events in RNA transcription. Moreover, it is ideal to reactivate PP2A in the SET-OE cells to further verify whether SET-induced hypertranscription or cell growth was mediated by PP2A inhibition; however, we did not achieve these results because phenothiazine-based PP2A-activating compounds iHAP1 and DT-061 had recently been found to have PP2A-independent cytotoxicity (*78*).

MATERIALS AND METHODS

Patient study

The paraffin section specimens were obtained from patients diagnosed with PDAC who underwent surgery at the Fudan University Shanghai Cancer Center (FUSCC) from 2016 to 2018. In the 239 patients, 104 had solely PDAC tissue, while the other 135 had both cancerous and adjacent tissue. PDAC RNA was extracted from the surgical tissues of 96 patients diagnosed in 2013 and 2014. Each patient provided an informed consent, and all experiments were conducted with the approval of the FUSCC Clinical Research Ethics Committee under the reference number 2109243-18. The disease diagnosis and IHC staining grading were performed by two experienced pathologists. The latest follow-up date was November 2020.

Cell lines and culture conditions

We cultured and passages HEK293T, *Drosophila* S2, mouse pancreatic cancer cell line Panc02, and human pancreatic cancer cell lines

BxPC3, Panc1, and MiaPaca2. The cells were identified by DNA fingerprinting. BxPC3 cells were cultured in RPMI 1640 supplemented with 10% fetal bovine serum (FBS). *Drosophila* S2 cells were maintained with Schneider's *Drosophila* medium with 10% FBS. The other cells were grown in Dulbecco's modified Eagle's medium with 10% FBS. All the media were supplemented with penicillin and streptomycin (100 U/ml). Cell lines were incubated at 37°C under 5% CO_2, and a PCR test for mycoplasma is performed every 2 months.

Mouse experiments

All animal experiments were conducted at the Animal Center of Fudan University Shanghai Cancer Center, and the Animal Ethics Committee approved the research with the reference number FUSCC-IACUC-2022125. A barrier system with ventilated cages and automatic water dispensers was used to house mice. The animal house is programmed with a temperature range of 20° to 26°C, a humidity range of 40 to 60%, and a 12-hour day/12-hour night cycle. Female BALB/c nude mice (5 to 6 weeks of age, 18 to 22 g; GemPharmatech) were injected subcutaneously with 1×10^6 BxPC3 control or SET-KO cells. The mice were euthanized, and the tumors were weighed 4 weeks after injection.

Immunohistochemistry

The IHC analysis was conducted in the same manner as previously described (*79*). Briefly, tissue sections with a thickness of 3 μm were deparaffinized in xylene and rehydrated in gradient alcohol solutions. Heat-mediated antigen retrieval was performed using EDTA buffer (pH 9.0) in a pressure cooker for 10 min. The slides were then cooled to room temperature and incubated with a 3% H_2O_2 solution for 20 min to inhibit endogenous peroxidase activity. After 2 hours of blocking with 3% normal goat serum, the slides were treated with optimum dilutions of primary antibodies at 4°C overnight. The samples were then stained using a two-step polymer–horseradish peroxidase method using DAB as the chromogen and Mayer's hematoxylin as the counterstain. Scores for IHC staining were calculated by multiplying the proportion or area (0, <5%; 1, 5 to 25%; 2, 25 to 50%; 3, 50 to 75%; and 4, >75%) of positively stained cells by the staining intensity (0, negative; 1, weak; 2, moderate; and 3, strong). Scores greater than six indicated high expression, whereas scores less than six indicated low expression.

Generation of KO and stably overexpression cell lines

The CRISPR-Cas9 technique was used to generate gene KOs. The annealed SET single guide RNA oligonucleotides were cloned into the pLentiCRISPR-V2 vector. Human full-length SET was inserted into the pLVX-Myc-puro vector (by Age-I and Eco RI). SET-KD or overexpression plasmids and virus packing plasmids were cotransfected into HEK293T cells to produce lenti-virus. The virus-containing supernatant was collected and purified after 48 hours, and BxPC3, Panc1, and Miapaca2 cells were then infected. The infected cells were selected with puromycin for 2 weeks. The genome sequence and Western blot were used to identify all the KO and overexpression cell lines.

siRNA knockdown

RNA interference transfections were carried out in a forward transfection mode using Lipofectamine 3000 transfection reagent according to the manufacturer's instructions. A total of 1×10^5 BxPC3 cells were seeded in 12-well plates before being transfected with a final small interfering RNA (siRNA) mixture of 20 nM and 2 μl of Lipofectamine per ml. Seventy-two hours after transfection, the cells were harvested for future experiments. KD efficiency was examined by Western blot.

Western blot

Cells were lysed in 1 × SDS–polyacrylamide gel electrophoresis (SDS-PAGE) loading buffer containing dithiothreitol (DTT) and incubated at 100°C for 10 min. β-Actin was used as a control for protein expression. All antibodies were determined experimentally and verified in the linear range. Samples were separated by SDS-PAGE (7.5 to 12.5%) and transferred onto the polyvinylidene difluoride (PVDF) membranes. The membranes of PVDF were blocked with a tris-buffered saline (TBS) buffer containing 0.1% Tween 20 and 5% non-fat milk or bovine serum albumin (BSA). Then, the membranes were treated overnight at 4°C with a primary antibody diluted in the blocking buffer. The next day, membranes were incubated at room temperature with secondary antibodies conjugated to HRP for 1 hour. The membrane was lastly constructed using a chemiluminescence substrate.

RNA extraction and RT-qPCR

Total RNA was extracted from clinical tumor specimens and human PDAC cells using an RNA extraction kit. The cDNA was synthesized from total RNA using the Prime Script RT Reagent Kit according to the manufacturer's instructions. The ΔΔCt technique was used to calculate relative mRNA expression levels, which were adjusted to β2M levels. ABI 7900HT Real-Time PCR machine (Applied Biosystems Inc., USA) was used for thermal cycling. The primers used are listed in table S2.

DNA site-specific mutation

The site-specific mutagenesis in the SET or Pp2ac CDS was generated by the PCR-based method. The primers are listed in table S2. Following the manufacturer's instructions, the KOD-Plus Mutagenesis Kit (Toyobo, Osaka, Japan) was used to generate mutant plasmids. All truncated mutations were confirmed by Sanger sequencing and expression in the HEK293T cells.

Cell viability assay

Cell viability was measured with the Cell Counting Kit-8 (CCK-8) following the manufacturer's instructions. In the 96-well plates, 3000 cells were inoculated per well overnight. The next day, 10 μl of CCK-8 solution were added to each well. After 90 min of incubation, the absorbance at 450 nm was measured with a microplate reader.

Cell death–detecting drug efficacy assay

Control and SET-KO BxPC3 cells were seeded in the 12-well plates and added gradient tivantinib after cells adhered. Twenty-four hours later, flow cytometric analysis was performed using the PE annexin V Apoptosis Detection Kit according to the manufacturer's instructions to determine cell apoptosis.

Immunoprecipitation-MS

A total of 1×10^7 HEK293T and Panc02 cells were stably transfected with the control and Myc-SET plasmids, respectively. Magnetic beads conjugated with anti-SET antibody were prewashed five times with 1× TBST buffer (25 mM tris, 0.15 M NaCl, and 0.05% Tween 20). Cells were washed three times with cold phosphate-buffered

saline (PBS) and then lysed in cell lysis buffer containing an EDTA-free protease inhibitor cocktail. The cell samples were added to the prewashed magnetic beads and incubated on a 4°C roller overnight. The beads were collected with magnetic stand and washed twice with 5× TBST buffer (125 mM tris, 0.75 M NaCl, and 0.25%Tween 20). A 50 μl of SDS-PAGE loading buffer was added, and the sample was incubated at 100°C for 10 min. The control SET and SET-OE–associated proteins were immunoprecipitated with magnetic beads and subjected to SDS-PAGE separation on 10% gel.

The protein gel strip was cut into pieces, and each piece was soaked for half an hour in sterile water in the corresponding EP tubes. The protein gel strip was decolorized at 37°C for 30 min or until the blue has faded and added acetonitrile to dehydrate the gel and make it completely white twice. The acetonitrile was soaked up and dried in the air. A 10 mM DTT was added until the liquid covers the gel, then placed it in a 56 °C water bath for 1 hour, placed it for 45 min in the dark after cooling to room temperature, and washed it twice with the decolorizing solution. The enzyme was diluted with 25 mM NH_4HCO_3 and placed on ice for 30 min. The appropriate buffer was added to the gel and incubated at 37°C overnight. The gel was washed with 50 and 100% ACN and took the supernatant to be freeze-dried. Thermo UltiMate 3000 UHPLC was used to separate samples of dried peptides. The liquid phase chromatography–separated peptides were ionized by a nanoESI source and passed to a tandem mass spectrometer Q-Exactive HF X for Data Dependent Acquisition mode detection.

CUT&Tag

The CUT&Tag assay was performed with minor modifications as previously described (*80*). The cells were gently washed three times with a wash buffer and incubated them with activated concanavalin A magnetic beads at room temperature for 10 min. The primary antibody was added and incubated on a rotating platform at 4°C overnight. The primary antibody was removed and incubated it for 30 min at room temperature on a rotating platform with diluted secondary antibodies. We washed it three times with Dig-Wash buffer and added 0.04 μM pA/G-Tnp for 1-hour rotated incubation. The cells were resuspended in TruePrep tagging buffer and incubated for 1 hour at 37°C. The DNA was purified with DNA extract beads. A 1 pg of *E. coli* genome DNA was added per 100,000 input cells for the spike-in control. Libraries were amplified using PCR according to the manufacturer's protocol. Following the manufacturer's recommendations, sequencing was carried out on an Illumina NovaSeq 6000 using 150–base pair (bp) paired-end.

Click-EU labeling nascent RNA

Cells were labeled with 5-EU for 2 hours before fixation and permeabilization. Then, cells were washed twice with 0.3% BSA in PBS and incubated at room temperature for 15 min with Click reaction buffer, CuSO4, Azide 488, and Click-IT additive solutons. Flow cytometry and imaging were performed on the treated cells.

Nascent RNA-seq

The nascent RNA-seq was performed with minor modifications as previously described (*24*, *81*). A total of 1×10^7 control and SET-KO cells were harvested with trypsin and washed with ice-cold PBS for three times. The cells were resuspend hypotonic buffer [10 mM Hepes (pH 7.9), 10 mM KCl, 2 mM $MgCl_2$, 1 mM DTT, and 1× protease inhibitor cocktail] and incubated for 20 min on ice. The suspension was centrifuged for 10 min at 4°C, and the supernantant was discarded. The cells were pulverized using a pestle to pulverize and ensure that 90% of the cells are broken up. The nuclei were collected by centrifuge at 600*g* for 10 min at 4°C. The nuclei was resuspended and washed with nuclei wash buffer [10 mM Hepes (pH 7.9), 250 mM sucrose, 1 mM DTT, 1 × protease inhibitor cocktail, ribonuclease inhibitor (50 U/ml)] twice. We mixed 50% volume of 2 M fresh urea solution and 50% volume of cold 2× NUN buffer [40 mM Hepes (pH 7.9), 15 mM $MgCl_2$, 600 mM NaCl, 0.4 mM EDTA, 2% (v/v) NP-40] with DTT for 1× NUN buffer. The pellet was suspended, and the nuclei was broken by pipetting up and down 10 to 15 times with 1 ml of 1 NUN buffer and incubated for 5 min at 4°C on a rotating plate. The chromatin was spun at 1000*g* for 3 min at 4°C to pelletize it. Also, the chromatin pellet was carefully resuspended in 1 × NUN buffer. The homogenized sample was incubated at 50°C for 5 min. The standard RNA purification protocol with TRIzol was followed for the remaining steps of RNA extraction.

The nascent RNA was detected with 1% agarose electrophoresis. The ribosomal RNA (rRNA) was purged, cDNA was synthesize, and libraries were constructed and amplified according to the manufacturer's guidelines. The quality of the library was validated using the Agilent DNA 1000 Kit on the Agilent 2100 Bioanalyzer. It was suitable to have smooth profiles peaking around 250 bp and no detectable primer dimer contamination. After 2 days of sequencing on an Illumina NovaSeq 6000 machine, the original data are lastly converted into Fastq format.

RNA-seq

RNA was isolated from control and SET-KO cells as previously described. On 0.8% agarose gels, RNA degradation and contamination were observed. The RNA sample preparations used a total of 3 μg of RNA as input material for each sample. Using the NEBNext Ultra-TM RNA Library Prep Kit for Illumina (NEB, USA) in accordance with the manufacturer's instructions, sequencing libraries were created, and index codes were added to assign sequences to specific samples. Biological triplicates of samples were sequenced using the Illumina NovaSeq6000 platform. HTSeq v0.6.0 was used to determine the number of reads mapped to each gene. The TPM of each gene was then evaluated on the basis of the gene's length and the total number of mapped reads.

ChIP-seq

Control and SET-KO cells were harvested for ChIP assay using validated ac-H4 or Pol II (Rpb1) NTD antibodies. Each group underwent two biological replicates of experiments. ChIP was performed based on the manufacturer's instructions using SimpleChIP Plus Enzymatic Chromatin IP Kit (Magnetic Beads). Specifically, approximately 5×10^6 cells were first fixed with 1% formaldehyde fixation. In each spike-in ChIP experiment, human cells were used in a 50:1 ratio to *Drosophila* S2 cells. At the start of the ChIP workflow, S2 cells were mixed in with human cells. After combining *Drosophila* S2 and human cells, the sample was treated as one ChIP-seq sample all across the experiment until the DNA sequencing was completed as described previously (*82*, *83*). The input and DNA samples were used to prepare sequencing libraries in accordance with the Illumina Genome Analyzer manufacturer's recommendations. After amplification, the total amount of DNA in each specimen was standardized. An Illumina NovaSeq 6000 Analyzer was used to sequence the purified.

PP2A immunoprecipitation phosphatase assay

For PP2A phosphatase assay, immunoprecipitations using lysates from six-well plate were performed according to the manufacturer's instructions. Briefly, the cells were washed with 1× TBS for three times, and the plates were scraped with 300 μl of phosphatase extraction buffer [20 mM imidazole-HCl, 2 mM EGTA, 2 mM EDTA, 1 mM benzamidine, 1× phenylmethylsulfonyl fluoride (pH 7.0), and 1× protease inhibitor cocktail]. The cells were sonicated for 10 s and centrifuged for 10 min at 2000*g* at 4°C. The tests for phosphatase activity were conducted using the isolated supernatant. PP2A-C antibody (clone 52F8D8, which recognizes both methylated and nonmethylated PP2A-C), Protein A agarose, and pNPP Ser/Thr assay buffer were added, then incubated constantly for 1 hour at 4°C on rocking plate, and washed and incubated with Ser/Thr assay buffer for 8 min at 30°C with shaking. Malachite green phosphate detection solution was added and read at 650 nm.

Quantification and statistical analysis

All replicate experiments were conducted using a minimum of two biological replicates per condition. According to the ENCODE project criteria, all the RNA-seq or nascent RNA-seq experiments in this research were performed with the samples of biological triplicates (three replicates), and all the ChIP-seq and Cut&Tag experiments are in duplicates (two replicates). Because the correlation coefficient between our replicates for each group is generally high, we would combine these replicate next generation sequencing (NGS) tracks into one merged (average) track to show in the figures for convenience. Generally, the statistical tests were performed after confirming that the data met appropriate assumptions (e.g., normal distribution) and two-tailed but nonparameter analysis is carried out if the distribution of assumptions could not be certified. *P* values were calculated and adjusted for multiple hypothesis testing where indicated. Statistical significance is indicated as $*P < 0.05$, $**P < 0.01$, and $***P < 0.001$. The statistical analyses were performed with R and GraphPad Prism. Pearson $\chi 2$ test or Fisher's exact test was used to examine categorical variables. Student's *t* test and Mann-Whitney–Wilcoxon test were used to analyze continuous variables. Survival comparisons were evaluated using Kaplan-Meier curves and log-rank tests. In RT-qPCR, relative gene expression levels normalized by β2M were calculated by the formula $2^{-\triangle Ct}$, where $\triangle Ct$ (critical threshold) = *C*t of genes of interest − Ct of β2M. In ChIP-qPCR, the enrichment for specific locus was normalized by input in the same way. Fold changes of gene expression level or ChIP enrichment were calculated by the $2^{-\triangle\triangle Ct}$ method. The data in histograms were presented as the means ± SD.

For the differential gene expression analysis method of the RNA-seq and the nascent RNA-seq data, first, the TPM of each gene was calculated using the sequencing data and based on the gene's length and the total number of mapped reads. The TPM values were then normalized according to the spike-in *Drosophila* S2 cell RNA, which was premixed in proportion with the total cell number. On the basis of the normalized TPM values for each gene in the control or SET-KO group (three replicates for each group), nonparameter analysis was performed to identify the DEGs.

Cell transcriptome connectivity matching

The Cell Connectivity Map (CMAP) is a compendium of gene expression signatures induced by chemical compounds or genetic perturbations (termed perturbagens) in multiple cell lines. For each small-molecule treatment or single gene knockdown/overexpression in a specific cell line, the L1000 assay platform measured the reduced representation of total transcriptome (~1000 land mark transcripts), recorded as an expression signature (*49*, *50*). CMAP has collected approximately 1.3 million expression signatures of more than 8000 perturbagens in at least seven cell types, and the "distance" between any two expression signatures is quantified using the Kolmogorov-Smirnov test. More similar expression signatures showed "shorter distance" and related higher "connectivity value." We searched CMAP (https://clue.io/) using the command: /conn "CDK9-OE". The resultant connectivity data were then downloaded and visualized as heatmaps.

Nascent RNA-seq analysis

Raw reads were trimmed and then aligned to human hg19 and *Drosophila* dm6 genome assemblies using STAR v2.7.5c with parameter "–outSAMtype BAM SortedByCoordinate–twopassMode Basic–outFilterMismatchNmax 2–outSJfilterReads Unique" (*84*). Read normalization was based on 1e6/spike-in read number calculated by SAMtools v1.9, and normalized bigWig files were built with deepTools v3.5.0 (*85*, *86*). Gene expression quantification was performed with featureCounts tool from the Rsubread R package v2.0.1 (*87*). For each gene, we computed the number of fragments per kilobase of exon per million mapped reads by normalizing the spike-in dm6 reads. Differential expression analysis was performed using DESeq2 R package v1.26.0 (*88*).

ChIP-seq analysis

The paired-end ChIP-seq reads were processed with Trim Galore v0.6.6 (www.bioinformatics.babraham.ac.uk/projects/trim_galore/) to remove adaptors and low-quality reads with the parameter "-q 25" and then aligned to the human hg19 and *Drosophila* dm6 assemblies using Bowtie v2.3.5.1 with default parameters (*89*). All unmapped reads, low mapping quality reads (MAPQ <30), and PCR duplicates were removed using SAMtools v1.9 (*85*) and Picard v2.23.3 (https://broadinstitute.github.io/picard/). The number of spike-in dm6 reads was counted with SAMtools v1.9, and normalization factor alpha = 1e6/dm6_count was calculated (*85*). Normalized bigWig was generated with deepTools v3.5.0, and reads mapped to the ENCODE blacklist regions were removed using bedtools v2.29.2 (*86*, *90*, *91*). Peaks were called using macs2 v2.2.6 with a *q* value threshold of 0.05, and peak annotation was performed with ChIPseeker R package v1.24.0 (*92*, *93*).

CUT&Tag analysis

Raw CUT&Tag reads were processed. CUT&Tag reads were trimmed using cutadapt (v1.16) (-m 10 -q 10). Paired-end reads were aligned to the hg19 reference genome using bowtie2 with default parameters. Normalized bigWig files were generated for each replicate using the bamCoverage function in the deepTools package. Replicates were further normalized to the input using the bigWigCompare function with the parameter-operation log.

Gene Ontology

Gene Ontology (GO) analysis was performed using the web interface for Database for Annotation, Visualization, and Integrated Discovery (DAVID, v.6.8). The Functional Annotation tool was used to identify biological process GO terms (GOTERM_BP_DIRECT)

that are enriched in the queried gene list. Selected GO terms with Benjamini-Hochberg–adjusted P value < 0.05 were plotted.

Data visualization

Reads per genomic content (RPGC)–normalized bigWig files were generated from ChIP-seq, CUT&Tag, nascent RNA-seq, and RNA-seq bam files using the BamCoverage function in the deepTools package (v.3.0.1) with parameters –normalizeUsing RPGC –effectiveGenomeSize 2652783500 –centerReads. For ChIP-seq and CUT&Tag data, the parameter –extendReads 150 was also used. RPGC-normalized ChIP-seq, CUT&Tag, nascent RNA-seq, and RNA-seq tracks at specific loci were visualized using Integrative Genomics Viewer (Broad Institute).

RPGC-normalized ChIP-seq and CUT&Tag signal was calculated in regions ±3 kb centered at the enhancer using the computeMatrix function in the deepTools package (reference-point –referencePoint center -a 3000, -b 3000 –binSize 10). Heatmaps and profiles of the signal were visualized using plotHeatmap and plotProfile functions, respectively, using default parameters (Figs. 2C and 5G and fig. S2B). Custom R code was used to generate profiles of mean signal from different samples at the same set of regions (Fig. 2E and fig. S7G).

Supplementary Materials

This PDF file includes:

Figs. S1 to S7
Tables S1 to S3

REFERENCES AND NOTES

1. S. B. Baylin, P. A. Jones, Epigenetic determinants of cancer. *Cold Spring Harb. Perspect. Biol.* **8**, a019505 (2016).
2. W. A. Flavahan, E. Gaskell, B. E. Bernstein, Epigenetic plasticity and the hallmarks of cancer. *Science* **357**, eaal2380 (2017).
3. D. Hanahan, Hallmarks of cancer: New dimensions. *Cancer Discov.* **12**, 31–46 (2022).
4. C. E. Nesbit, J. M. Tersak, E. V. Prochownik, MYC oncogenes and human neoplastic disease. *Oncogene* **18**, 3004–3016 (1999).
5. N. Meyer, L. Z. Penn, Reflecting on 25 years with MYC. *Nat. Rev. Cancer* **8**, 976–990 (2008).
6. C. Y. Lin, J. Lovén, P. B. Rahl, R. M. Paranal, C. B. Burge, J. E. Bradner, T. I. Lee, R. A. Young, Transcriptional amplification in tumor cells with elevated c-Myc. *Cell* **151**, 56–67 (2012).
7. B. Chapuy, M. R. McKeown, C. Y. Lin, S. Monti, M. G. Roemer, J. Qi, P. B. Rahl, H. H. Sun, K. T. Yeda, J. G. Doench, E. Reichert, A. L. Kung, S. J. Rodig, R. A. Young, M. A. Shipp, J. E. Bradner, Discovery and characterization of super-enhancer-associated dependencies in diffuse large B cell lymphoma. *Cancer Cell* **24**, 777–790 (2013).
8. D. Hnisz, B. J. Abraham, T. I. Lee, A. Lau, V. Saint-André, A. A. Sigova, H. A. Hoke, R. A. Young, Super-enhancers in the control of cell identity and disease. *Cell* **155**, 934–947 (2013).
9. J. Lovén, H. A. Hoke, C. Y. Lin, A. Lau, D. A. Orlando, C. R. Vakoc, J. E. Bradner, T. I. Lee, R. A. Young, Selective inhibition of tumor oncogenes by disruption of super-enhancers. *Cell* **153**, 320–334 (2013).
10. E. Chipumuro, E. Marco, C. L. Christensen, N. Kwiatkowski, T. Zhang, C. M. Hatheway, B. J. Abraham, B. Sharma, C. Yeung, A. Altabef, A. Perez-Atayde, K. K. Wong, G. C. Yuan, N. S. Gray, R. A. Young, R. E. George, CDK7 inhibition suppresses super-enhancer-linked oncogenic transcription in MYCN-driven cancer. *Cell* **159**, 1126–1139 (2014).
11. C. L. Christensen, N. Kwiatkowski, B. J. Abraham, J. Carretero, F. Al-Shahrour, T. Zhang, E. Chipumuro, G. S. Herter-Sprie, E. A. Akbay, A. Altabef, J. Zhang, T. Shimamura, M. Capelletti, J. B. Reibel, J. D. Cavanaugh, P. Gao, Y. Liu, S. R. Michaelsen, H. S. Poulsen, A. R. Aref, D. A. Barbie, J. E. Bradner, R. E. George, N. S. Gray, R. A. Young, K. K. Wong, Targeting transcriptional addictions in small cell lung cancer with a covalent CDK7 inhibitor. *Cancer Cell* **26**, 909–922 (2014).
12. N. Kwiatkowski, T. Zhang, P. B. Rahl, B. J. Abraham, J. Reddy, S. B. Ficarro, A. Dastur, A. Amzallag, S. Ramaswamy, B. Tesar, C. E. Jenkins, N. M. Hannett, D. McMillin, T. Sanda, T. Sim, N. D. Kim, T. Look, C. S. Mitsiades, A. P. Weng, J. R. Brown, C. H. Benes, J. A. Marto, R. A. Young, N. S. Gray, Targeting transcription regulation in cancer with a covalent CDK7 inhibitor. *Nature* **511**, 616–620 (2014).
13. M. R. Mansour, B. J. Abraham, L. Anders, A. Berezovskaya, A. Gutierrez, A. D. Durbin, J. Etchin, L. Lawton, S. E. Sallan, L. B. Silverman, M. L. Loh, S. P. Hunger, T. Sanda, R. A. Young, A. T. Look, Oncogene regulation. An oncogenic super-enhancer formed through somatic mutation of a noncoding intergenic element. *Science* **346**, 1373–1377 (2014).
14. S. Sengupta, R. E. George, Super-enhancer-driven transcriptional dependencies in cancer. *Trends Cancer* **3**, 269–281 (2017).
15. P. Thandapani, Super-enhancers in cancer. *Pharmacol. Ther* **199**, 129–138 (2019).
16. B. M. Peterlin, D. H. Price, Controlling the elongation phase of transcription with P-TEFb. *Mol. Cell* **23**, 297–305 (2006).
17. Q. Zhou, T. Li, D. H. Price, RNA polymerase II elongation control. *Annu. Rev. Biochem.* **81**, 119–143 (2012).
18. B. L. Allen, D. J. Taatjes, The Mediator complex: A central integrator of transcription. *Nat. Rev. Mol. Cell Biol.* **16**, 155–166 (2015).
19. I. Jonkers, J. T. Lis, Getting up to speed with transcription elongation by RNA polymerase II. *Nat. Rev. Mol. Cell Biol.* **16**, 167–177 (2015).
20. H. Lu, Y. Xue, G. K. Yu, C. Arias, J. Lin, S. Fong, M. Faure, B. Weisburd, X. Ji, A. Mercier, J. Sutton, K. Luo, Z. Gao, Q. Zhou, Compensatory induction of MYC expression by sustained CDK9 inhibition via a BRD4-dependent mechanism. *eLife* **4**, e06535 (2015).
21. P. Filippakopoulos, J. Qi, S. Picaud, Y. Shen, W. B. Smith, O. Fedorov, E. M. Morse, T. Keates, T. T. Hickman, I. Felletar, M. Philpott, S. Munro, M. R. McKeown, Y. Wang, A. L. Christie, N. West, M. J. Cameron, B. Schwartz, T. D. Heightman, N. La Thangue, C. A. French, O. Wiest, A. L. Kung, S. Knapp, J. E. Bradner, Selective inhibition of BET bromodomains. *Nature* **468**, 1067–1073 (2010).
22. J. S. Roe, F. Mercan, K. Rivera, D. J. Pappin, C. R. Vakoc, BET bromodomain inhibition suppresses the function of hematopoietic transcription factors in acute myeloid leukemia. *Mol. Cell* **58**, 1028–1039 (2015).
23. Y. Yan, J. Ma, D. Wang, D. Lin, X. Pang, S. Wang, Y. Zhao, L. Shi, H. Xue, Y. Pan, J. Zhang, C. Wahlestedt, F. J. Giles, Y. Chen, M. E. Gleave, C. C. Collins, D. Ye, Y. Wang, H. Huang, The novel BET-CBP/p300 dual inhibitor NEO2734 is active in SPOP mutant and wild-type prostate cancer. *EMBO Mol. Med.* **11**, e10659 (2019).
24. H. Zheng, Y. Qi, S. Hu, X. Cao, C. Xu, Z. Yin, X. Chen, Y. Li, W. Liu, J. Li, J. Wang, G. Wei, K. Liang, F. X. Chen, Y. Xu, Identification of integrator-PP2A complex (INTAC), an RNA polymerase II phosphatase. *Science* **370**, eabb5872 (2020).
25. S. J. Vervoort, S. A. Welsh, J. R. Devlin, E. Barbieri, D. A. Knight, S. Offley, S. Bjelosevic, M. Costacurta, I. Todorovski, C. J. Kearney, J. J. Sandow, Z. Fan, B. Blyth, V. McLeod, J. H. A. Vissers, K. Pavic, B. P. Martin, G. Gregory, E. Demosthenous, M. Zethoven, I. Y. Kong, E. D. Hawkins, S. J. Hogg, M. J. Kelly, A. Newbold, K. J. Simpson, O. Kauko, K. F. Harvey, M. Ohlmeyer, J. Westermarck, N. Gray, A. Gardini, R. W. Johnstone, The PP2A-Integrator-CDK9 axis fine-tunes transcription and can be targeted therapeutically in cancer. *Cell* **184**, 3143–3162.e32 (2021).
26. M. Tellier, J. Zaborowska, J. Neve, T. Nojima, S. Hester, M. Fournier, A. Furger, S. Murphy, CDK9 and PP2A regulate RNA polymerase II transcription termination and coupled RNA maturation. *EMBO Rep.* **23**, e54520 (2022).
27. K. Matsumoto, M. Okuwaki, H. Kawase, H. Handa, F. Hanaoka, K. Nagata, Stimulation of DNA transcription by the replication factor from the adenovirus genome in a chromatin-like structure. *J. Biol. Chem.* **270**, 9645–9650 (1995).
28. M. Okuwaki, K. Nagata, Template activating factor-I remodels the chromatin structure and stimulates transcription from the chromatin template. *J. Biol. Chem.* **273**, 34511–34518 (1998).
29. M. J. Gamble, H. Erdjument-Bromage, P. Tempst, L. P. Freedman, R. P. Fisher, The histone chaperone TAF-I/SET/INHAT is required for transcription in vitro of chromatin templates. *Mol. Cell. Biol.* **25**, 797–807 (2005).
30. S. B. Seo, P. McNamara, S. Heo, A. Turner, W. S. Lane, D. Chakravarti, Regulation of histone acetylation and transcription by INHAT, a human cellular complex containing the set oncoprotein. *Cell* **104**, 119–130 (2001).
31. M. Li, A. Makkinje, Z. Damuni, The myeloid leukemia-associated protein SET is a potent inhibitor of protein phosphatase 2A. *J. Biol. Chem.* **271**, 11059–11062 (1996).
32. S. Saito, M. Miyaji-Yamaguchi, T. Shimoyama, K. Nagata, Functional domains of template-activating factor-I as a protein phosphatase 2A inhibitor. *Biochem. Biophys. Res. Commun.* **259**, 471–475 (1999).
33. R. Trotta, D. Ciarlariello, J. Dal Col, J. Allard II, P. Neviani, R. Santhanam, H. Mao, B. Becknell, J. Yu, A. K. Ferketich, B. Thomas, A. Modi, B. W. Blaser, D. Perrotti, M. A. Caligiuri, The PP2A inhibitor SET regulates natural killer cell IFN-gamma production. *J. Exp. Med.* **204**, 2397–2405 (2007).
34. P. Neviani, R. Santhanam, R. Trotta, M. Notari, B. W. Blaser, S. Liu, H. Mao, J. S. Chang, A. Galietta, A. Uttam, D. C. Roy, M. Valtieri, R. Bruner-Klisovic, M. A. Caligiuri, C. D. Bloomfield, G. Marcucci, D. Perrotti, The tumor suppressor PP2A is functionally inactivated in blast crisis CML through the inhibitory activity of the BCR/ABL-regulated SET protein. *Cancer Cell* **8**, 355–368 (2005).
35. M. Li, H. Guo, Z. Damuni, Purification and characterization of two potent heat-stable protein inhibitors of protein phosphatase 2A from bovine kidney. *Biochemistry* **34**, 1988–1996 (1995).

36. Y. C. Chae, K. B. Kim, J. Y. Kang, S. R. Kim, H. S. Jung, S. B. Seo, Inhibition of FoxO1 acetylation by INHAT subunit SET/TAF-Iβ induces p21 transcription. *FEBS Lett.* **588**, 2867–2873 (2014).
37. D. Wang, N. Kon, G. Lasso, L. Jiang, W. Leng, W. G. Zhu, J. Qin, B. Honig, W. Gu, Acetylation-regulated interaction between p53 and SET reveals a widespread regulatory mode. *Nature* **538**, 118–122 (2016).
38. A. Kalousi, A. S. Hoffbeck, P. N. Selemenakis, J. Pinder, K. I. Savage, K. K. Khanna, L. Brino, G. Dellaire, V. G. Gorgoulis, E. Soutoglou, The nuclear oncogene SET controls DNA repair by KAP1 and HP1 retention to chromatin. *Cell Rep.* **11**, 149–163 (2015).
39. R. R. Edupuganti, A. Harikumar, Y. Aaronson, A. Biran, B. S. Sailaja, M. Nissim-Rafinia, G. K. Azad, M. A. Cohen, J. E. Park, C. S. Shivalila, S. Markoulaki, S. K. Sze, R. Jaenisch, E. Meshorer, Alternative SET/TAFI Promoters Regulate Embryonic Stem Cell Differentiation. *Stem Cell Rep.* **9**, 1291–1303 (2017).
40. S. Krishnan, A. H. Smits, M. Vermeulen, D. Reinberg, Phospho-H1 decorates the inter-chromatid axis and is evicted along with shugoshin by SET during mitosis. *Mol. Cell* **67**, 579–593.e6 (2017).
41. Y. Asai, R. Matsumura, Y. Hasumi, H. Susumu, K. Nagata, Y. Watanabe, Y. Terada, SET/TAF1 forms a distance-dependent feedback loop with Aurora B and Bub1 as a tension sensor at centromeres. *Sci. Rep.* **10**, 15653 (2020).
42. M. Miyaji-Yamaguchi, M. Okuwaki, K. Nagata, Coiled-coil structure-mediated dimerization of template activating factor-I is critical for its chromatin remodeling activity. *J. Mol. Biol.* **290**, 547–557 (1999).
43. H. Haruki, M. Okuwaki, M. Miyagishi, K. Taira, K. Nagata, Involvement of template-activating factor I/SET in transcription of adenovirus early genes as a positive-acting factor. *J. Virol.* **80**, 794–801 (2006).
44. K. Kato, M. Miyaji-Yamaguchi, M. Okuwaki, K. Nagata, Histone acetylation-independent transcription stimulation by a histone chaperone. *Nucleic Acids Res.* **35**, 705–715 (2007).
45. Z. Fan, P. J. Beresford, D. Y. Oh, D. Zhang, J. Lieberman, Tumor suppressor NM23-H1 is a granzyme A-activated DNase during CTL-mediated apoptosis, and the nucleosome assembly protein SET is its inhibitor. *Cell* **112**, 659–672 (2003).
46. K. Matsumoto, K. Nagata, M. Miyaji-Yamaguchi, A. Kikuchi, M. Tsujimoto, Sperm chromatin decondensation by template activating factor I through direct interaction with basic proteins. *Mol. Cell. Biol.* **19**, 6940–6952 (1999).
47. N. Cervoni, N. Detich, S. B. Seo, D. Chakravarti, M. Szyf, The oncoprotein Set/TAF-1beta, an inhibitor of histone acetyltransferase, inhibits active demethylation of DNA, integrating DNA methylation and transcriptional silencing. *J. Biol. Chem.* **277**, 25026–25031 (2002).
48. Z. Karetsou, G. Martic, S. Tavoulari, S. Christoforidis, M. Wilm, C. Gruss, T. Papamarcaki, Prothymosin alpha associates with the oncoprotein SET and is involved in chromatin decondensation. *FEBS Lett.* **577**, 496–500 (2004).
49. J. Lamb, E. D. Crawford, D. Peck, J. W. Modell, I. C. Blat, M. J. Wrobel, J. Lerner, J. P. Brunet, A. Subramanian, K. N. Ross, M. Reich, H. Hieronymus, G. Wei, S. A. Armstrong, S. J. Haggarty, P. A. Clemons, R. Wei, S. A. Carr, E. S. Lander, T. R. Golub, The Connectivity Map: Using gene-expression signatures to connect small molecules, genes, and disease. *Science* **313**, 1929–1935 (2006).
50. A. Subramanian, R. Narayan, S. M. Corsello, D. D. Peck, T. E. Natoli, X. Lu, J. Gould, J. F. Davis, A. A. Tubelli, J. K. Asiedu, D. L. Lahr, J. E. Hirschman, Z. Liu, M. Donahue, B. Julian, M. Khan, D. Wadden, I. C. Smith, D. Lam, A. Liberzon, C. Toder, M. Bagul, M. Orzechowski, O. M. Enache, F. Piccioni, S. A. Johnson, N. J. Lyons, A. H. Berger, A. F. Shamji, A. N. Brooks, A. Vrcic, C. Flynn, J. Rosains, D. Y. Takeda, R. Hu, D. Davison, J. Lamb, K. Ardlie, L. Hogstrom, P. Greenside, N. S. Gray, P. A. Clemons, S. Silver, X. Wu, W. N. Zhao, W. Read-Button, X. Wu, S. J. Haggarty, L. V. Ronco, J. S. Boehm, S. L. Schreiber, J. G. Doench, J. A. Bittker, D. E. Root, B. Wong, T. R. Golub, A next generation connectivity Map: L1000 Platform and the First 1,000,000 Profiles. *Cell* **171**, 1437–1452.e17 (2017).
51. L. Arnaud, S. Chen, F. Liu, B. Li, S. Khatoon, I. Grundke-Iqbal, K. Iqbal, Mechanism of inhibition of PP2A activity and abnormal hyperphosphorylation of tau by I2(PP2A)/SET. *FEBS Lett.* **585**, 2653–2659 (2011).
52. R. M. De Palma, S. R. Parnham, Y. Li, J. J. Oaks, Y. K. Peterson, Z. M. Szulc, B. M. Roth, Y. Xing, B. Ogretmen, The NMR-based characterization of the FTY720-SET complex reveals an alternative mechanism for the attenuation of the inhibitory SET-PP2A interaction. *FASEB J.* **33**, 7647–7666 (2019).
53. S. A. Saddoughi, S. Gencer, Y. K. Peterson, K. E. Ward, A. Mukhopadhyay, J. Oaks, J. Bielawski, Z. M. Szulc, R. J. Thomas, S. P. Selvam, C. E. Senkal, E. Garrett-Mayer, R. M. De Palma, D. Fedarovich, A. Liu, A. A. Habib, R. V. Stahelin, D. Perrotti, B. Ogretmen, Sphingosine analogue drug FTY720 targets I2PP2A/SET and mediates lung tumour suppression via activation of PP2A-RIPK1-dependent necroptosis. *EMBO Mol. Med.* **5**, 105–121 (2013).
54. Y. Shi, Serine/threonine phosphatases: Mechanism through structure. *Cell* **139**, 468–484 (2009).
55. K. Pavic, N. Gupta, J. D. Omella, R. Derua, A. Aakula, R. Huhtaniemi, J. A. Määttä, N. Höfflin, J. Okkeri, Z. Wang, O. Kauko, R. Varjus, H. Honkanen, D. Abankwa, M. Köhn, V. P. Hytönen, W. Xu, J. Nilsson, R. Page, V. Janssens, A. Leitner, J. Westermarck, Structural mechanism for inhibition of PP2A-B56α and oncogenicity by CIP2A. *Nat. Commun.* **14**, 1143 (2023).
56. O. Kauko, S. Y. Imanishi, E. Kulesskiy, L. Yetukuri, T. D. Laajala, M. Sharma, K. Pavic, A. Aakula, C. Rupp, M. Jumppanen, P. Haapaniemi, L. Ruan, B. Yadav, V. Suni, T. Varila, G. L. Corthals, J. Reimand, K. Wennerberg, T. Aittokallio, J. Westermarck, Phosphoproteome and drug-response effects mediated by the three protein phosphatase 2A inhibitor proteins CIP2A, SET, and PME-1. *J. Biol. Chem.* **295**, 4194–4211 (2020).
57. H. T. Adler, F. S. Nallaseth, G. Walter, D. C. Tkachuk, HRX leukemic fusion proteins form a heterocomplex with the leukemia-associated protein SET and protein phosphatase 2A. *J. Biol. Chem.* **272**, 28407–28414 (1997).
58. D. J. Christensen, Y. Chen, J. Oddo, K. M. Matta, J. Neil, E. D. Davis, A. D. Volkheimer, M. C. Lanasa, D. R. Friedman, B. K. Goodman, J. P. Gockerman, L. F. Diehl, C. M. de Castro, J. O. Moore, M. P. Vitek, J. B. Weinberg, SET oncoprotein overexpression in B-cell chronic lymphocytic leukemia and non-Hodgkin lymphoma: A predictor of aggressive disease and a new treatment target. *Blood* **118**, 4150–4158 (2011).
59. M. P. Menden, F. P. Casale, J. Stephan, G. R. Bignell, F. Iorio, U. McDermott, M. J. Garnett, J. Saez-Rodriguez, O. Stegle, The germline genetic component of drug sensitivity in cancer cell lines. *Nat. Commun.* **9**, 3385 (2018).
60. M. Ebert, M. Yokoyama, H. Friess, M. W. Büchler, M. Korc, Coexpression of the c-met proto-oncogene and hepatocyte growth factor in human pancreatic cancer. *Cancer Res.* **54**, 5775–5778 (1994).
61. K. Kiehne, K. H. Herzig, U. R. Fölsch, c-met expression in pancreatic cancer and effects of hepatocyte growth factor on pancreatic cancer cell growth. *Pancreas* **15**, 35–40 (1997).
62. K. H. Lee, M. S. Hyun, J. R. Kim, Invasion-metastasis by hepatocyte growth factor/c-met signaling concomitant with induction of urokinase plasminogen activator in human pancreatic cancer: Role as therapeutic target. *Cancer Res. Treat.* **35**, 207–212 (2003).
63. B. Yan, Z. Jiang, L. Cheng, K. Chen, C. Zhou, L. Sun, W. Qian, J. Li, J. Cao, Q. Xu, Q. Ma, J. Lei, Paracrine HGF/c-MET enhances the stem cell-like potential and glycolysis of pancreatic cancer cells via activation of YAP/HIF-1α. *Exp. Cell Res.* **371**, 63–71 (2018).
64. T. Qin, Y. Xiao, W. Qian, X. Wang, M. Gong, Q. Wang, R. An, L. Han, W. Duan, Q. Ma, Z. Wang, HGF/c-Met pathway facilitates the perineural invasion of pancreatic cancer by activating the mTOR/NGF axis. *Cell Death Dis.* **13**, 387 (2022).
65. S. Larochelle, R. Amat, K. Glover-Cutter, M. Sansó, C. Zhang, J. J. Allen, K. M. Shokat, D. L. Bentley, R. P. Fisher, Cyclin-dependent kinase control of the initiation-to-elongation switch of RNA polymerase II. *Nat. Struct. Mol. Biol.* **19**, 1108–1115 (2012).
66. D. Eick, M. Geyer, The RNA polymerase II carboxy-terminal domain (CTD) code. *Chem. Rev.* **113**, 8456–8490 (2013).
67. M. J. Gamble, R. P. Fisher, SET and PARP1 remove DEK from chromatin to permit access by the transcription machinery. *Nat. Struct. Mol. Biol.* **14**, 548–555 (2007).
68. S. Muto, M. Senda, Y. Akai, L. Sato, T. Suzuki, R. Nagai, T. Senda, M. Horikoshi, Relationship between the structure of SET/TAF-Ibeta/INHAT and its histone chaperone activity. *Proc. Natl. Acad. Sci. U.S.A.* **104**, 4285–4290 (2007).
69. Y. Kitajima, T. Ide, T. Ohtsuka, K. Miyazaki, Induction of hepatocyte growth factor activator gene expression under hypoxia activates the hepatocyte growth factor/c-Met system via hypoxia inducible factor-1 in pancreatic cancer. *Cancer Sci.* **99**, 1341–1347 (2008).
70. K. Noguchi, M. Konno, H. Eguchi, K. Kawamoto, R. Mukai, N. Nishida, J. Koseki, H. Wada, H. Akita, T. Satoh, S. Marubashi, H. Nagano, Y. Doki, M. Mori, H. Ishii, c-Met affects gemcitabine resistance during carcinogenesis in a mouse model of pancreatic cancer. *Oncol. Lett.* **16**, 1892–1898 (2018).
71. A. Lux, C. Kahlert, R. Grützmann, C. Pilarsky, c-Met and PD-L1 on circulating exosomes as diagnostic and prognostic markers for pancreatic cancer. *Int. J. Mol. Sci.* **20**, (2019).
72. H. Jin, R. Yang, Z. Zheng, M. Romero, J. Ross, H. Bou-Reslan, R. A. Carano, I. Kasman, E. Mai, J. Young, J. Zha, Z. Zhang, S. Ross, R. Schwall, G. Colbern, M. Merchant, MetMAb, the one-armed 5D5 anti-c-Met antibody, inhibits orthotopic pancreatic tumor growth and improves survival. *Cancer Res.* **68**, 4360–4368 (2008).
73. C. Li, J. J. Wu, M. Hynes, J. Dosch, B. Sarkar, T. H. Welling, M. Pasca di Magliano, D. M. Simeone, c-Met is a marker of pancreatic cancer stem cells and therapeutic target. *Gastroenterology* **141**, 2218–2227.e5 (2011).
74. M. Herreros-Villanueva, A. Zubia-Olascoaga, L. Bujanda, c-Met in pancreatic cancer stem cells: Therapeutic implications. *World J. Gastroenterol.* **18**, 5321–5323 (2012).
75. Y. Jin, Z. Zhang, S. Zou, F. Li, H. Chen, C. Peng, X. Deng, C. Wen, B. Shen, Q. Zhan, A Novel c-MET-targeting antibody-drug conjugate for pancreatic cancer. *Front. Oncol.* **11**, 634881 (2021).
76. S. Mori, H. Akita, S. Kobayashi, Y. Iwagami, D. Yamada, Y. Tomimaru, T. Noda, K. Gotoh, Y. Takeda, M. Tanemura, Y. Doki, H. Eguchi, Inhibition of c-MET reverses radiation-induced malignant potential in pancreatic cancer. *Cancer Lett.* **512**, 51–59 (2021).
77. A. Aakula, M. Sharma, F. Tabaro, R. Nätkin, J. Kamila, H. Honkanen, M. Schapira, C. Arrowsmith, M. Nykter, J. Westermarck, RAS and PP2A activities converge on epigenetic gene regulation. *Life Sci Alliance* **6**, e202301928 (2023).

78. G. Vit, J. Duro, G. Rajendraprasad, E. P. T. Hertz, L. K. K. Holland, M. B. Weisser, B. C. McEwan, B. Lopez-Mendez, P. Sotelo-Parrilla, A. A. Jeyaprakash, G. Montoya, N. Mailand, K. Maeda, A. Kettenbach, M. Barisic, J. Nilsson, Chemogenetic profiling reveals PP2A-independent cytotoxicity of proposed PP2A activators iHAP1 and DT-061. *EMBO J.* **41**, e110611 (2022).
79. J. Hua, S. Shi, J. Xu, M. Wei, Y. Zhang, J. Liu, B. Zhang, X. Yu, Expression patterns and prognostic value of DNA damage repair proteins in resected pancreatic neuroendocrine neoplasms. *Ann. Surg.* **275**, e443–e452 (2022).
80. H. S. Kaya-Okur, S. J. Wu, C. A. Codomo, E. S. Pledger, T. D. Bryson, J. G. Henikoff, K. Ahmad, S. Henikoff, CUT&Tag for efficient epigenomic profiling of small samples and single cells. *Nat. Commun.* **10**, 1930 (2019).
81. F. X. Chen, S. A. Marshall, Y. Deng, S. Tianjiao, Measuring Nascent Transcripts by Nascent-seq. Methods in molecular biology (Clifton, N.J.) 1712, 19–26 (2018).
82. D. Wu, L. Wang, H. Huang, Protocol to apply spike-in ChIP-seq to capture massive histone acetylation in human cells. *STAR Protoc* **2**, 100681 (2021).
83. D. Wu, Y. Yan, T. Wei, Z. Ye, Y. Xiao, Y. Pan, J. J. Orme, D. Wang, L. Wang, S. Ren, H. Huang, An acetyl-histone vulnerability in PI3K/AKT inhibition-resistant cancers is targetable by both BET and HDAC inhibitors. *Cell Rep.* **34**, 108744 (2021).
84. A. Dobin, C. A. Davis, F. Schlesinger, J. Drenkow, C. Zaleski, S. Jha, P. Batut, M. Chaisson, T. R. Gingeras, STAR: Ultrafast universal RNA-seq aligner. *Bioinformatics* **29**, 15–21 (2013).
85. H. Li, B. Handsaker, A. Wysoker, T. Fennell, J. Ruan, N. Homer, G. Marth, G. Abecasis, R. Durbin, The Sequence Alignment/Map format and SAMtools. *Bioinformatics* **25**, 2078–2079 (2009).
86. F. Ramírez, D. P. Ryan, B. Grüning, V. Bhardwaj, F. Kilpert, A. S. Richter, S. Heyne, F. Dündar, T. Manke, deepTools2: A next generation web server for deep-sequencing data analysis. *Nucleic Acids Res.* **44**, W160–W165 (2016).
87. Y. Liao, G. K. Smyth, W. Shi, The R package Rsubread is easier, faster, cheaper and better for alignment and quantification of RNA sequencing reads. *Nucleic Acids Res.* **47**, e47 (2019).
88. M. I. Love, W. Huber, S. Anders, Moderated estimation of fold change and dispersion for RNA-seq data with DESeq2. *Genome Biol.* **15**, 550 (2014).
89. B. Langmead, S. L. Salzberg, Fast gapped-read alignment with Bowtie 2. *Nat. Methods* **9**, 357–359 (2012).
90. A. R. Quinlan, I. M. Hall, BEDTools: A flexible suite of utilities for comparing genomic features. *Bioinformatics* **26**, 841–842 (2010).
91. H. M. Amemiya, A. Kundaje, A. P. Boyle, The ENCODE Blacklist: Identification of problematic regions of the genome. *Sci. Rep.* **9**, 9354 (2019).
92. Y. Zhang, T. Liu, C. A. Meyer, J. Eeckhoute, D. S. Johnson, B. E. Bernstein, C. Nusbaum, R. M. Myers, M. Brown, W. Li, X. S. Liu, Model-based analysis of ChIP-Seq (MACS). *Genome Biol.* **9**, R137 (2008).
93. G. Yu, L. G. Wang, Q. Y. He, ChIPseeker: An R/Bioconductor package for ChIP peak annotation, comparison and visualization. *Bioinformatics* **31**, 2382–2383 (2015).

Acknowledgments: We thank X. Wu of the Westlake University for the SET-PP2AC complex structure simulation and F. Xavier Chen of the Fudan University Shanghai Cancer Center for sharing of nascent RNA-seq technology. **Funding:** This work was funded by National Natural Science Foundation of China (U21A20374, 82072698, 82002541, and 82203434), China Post-Doc Science Foundation (2021 M690698), Shanghai Municipal Science and Technology Major Project (21JC1401500), Scientific Innovation Project of Shanghai Education Committee (2019-01-07-00-07-E00057), Clinical Research Plan of Shanghai Hospital Development Center (SHDC2020CR1006A), Xuhui District Artificial Intelligence Medical Hospital Cooperation Project (2021-011), and Shanghai Rising-Star Program (no. 20QA1402100). **Author contributions:** D.W. and S.S. conceptualized the study. D.W. and H.X. found the connectivity between SET overexpression and CDK9 gain of function, as well as the positive effect of SET upon Pol II–mediated transcription and super-enhancer activation. H.X. performed patient studies, cell culture, and animal experiments. D.W. H.X., M.X., and Yubin Lei. performed the nascent RNA-seq, RNA-seq, ChIP-seq, and CUT&Tag. D.W. performed the computational analysis. Yalan Lei drawn the heatmaps of RNA-seq. D.W. wrote the manuscript. D.W., X.Y., and S.S. supervised the work. **Competing interests:** The authors declare that they have no competing interests. **Data and materials availability:** Further information and requests for resources and reagents should be directed to S.S. (shisi@fudanpci.org). Cell lines and plasmids are listed in the table S1. Oligonucleotides are listed in table S2. All sequencing tracks generated from nascent RNA-seq, RNA-seq, ChIP-seq, and CUT&Tag reported here and gene expression TPM lists have been deposited to Mendeley Data (https://data.mendeley.com/datasets/ys5kswxvw7/draft?a=3f82e213-d935-4e74-b88c-f5968b9417a1) along with the original Western blot images and the IP-MS data to the Dryad (https://doi.org/10.5061/dryad.9p8cz8wpr). Table S3 shows the relationship between the raw sequencing data and the derived figure results. All data needed to evaluate the conclusions in the paper are present in the paper and/or the Supplementary Materials.

Submitted 4 September 2023
Accepted 26 December 2023
Published 26 January 2024
10.1126/sciadv.adk6633